

# Model Order Reduction Techniques for PEEC Modeling of RF&High-speed Multi-layer Circuits

by



HU Hai

A Thesis Submitted in Partial Fulfillment of the  
Requirement for the Degree of  
Master of Philosophy  
in  
Electronic Engineering

©The Chinese University of Hong Kong  
August 2006

The Chinese University of Hong Kong holds the copyright of this thesis. Any person(s) intending to use a part or whole of the materials in the thesis in a proposed publication must seek copyright release from the Dean of the Graduate School.

Model Order Reduction Techniques for  
FEM Modelling of RVE High-order  
Multi-layer Composites



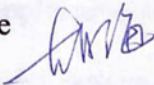
The Chinese University of Hong Kong Library System  
part of the University of Hong Kong  
Library System

## Author's Declaration

I hereby declare that I am the sole author of this thesis.

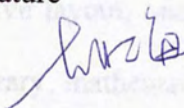
I authorize the Chinese University of Hong Kong to lend this thesis to other institutions or individuals for the purpose of scholarly research.

Signature



I further authorize the Chinese University of Hong Kong to reproduce this thesis by photocopying or by other means, in total or in part, at the request of other institutions or individuals for the purpose of scholarly research.

Signature



## Abstract

With the increasing of operating frequency, the inevitable parasitic effects have become a major problem challenging the designers in RF industry. By far, many electronic design automatic (EDA) tools have incorporated algorithms for estimating and calculating the parasitics. Partial Element Electronic Circuit (PEEC) is one of the choices. PEEC converts a distributed layout design into a circuit schematic, in which RF layout with interconnects are expressed by resistances, capacitances and inductances with mutual couplings linking with each other. However, even though PEEC algorithm has facilitated RF design process, the complexity of the resultant circuit model could greatly hinder PEEC's extensive application on more complicated layout over high frequency range. Hence we need model order reduction (MOR) to simplify the obtained circuit networks. In recent years, MOR has become a very popular topic in RF computer aided design realm.

In this work, two categories of MOR techniques have been investigated. The first is the so-called mathematical MOR, where the original circuit domain variables are all packed into matrices-expressed state-space equations, and then this large state-space is projected to a much smaller state-space which can preserve the major input-output features of the original circuit. The second is the so-called physical MOR, where the original circuit is reduced node by node following a certain simplification sequence that least affects the main attributes of the original network.

The main concern in this thesis is the physical MOR on circuits generated from a lossy RF passive layout, because after physical MOR, more concise circuit can be obtained. On the contrary, mathematical MOR model cannot give back a circuit domain model with physical

meaning, thus it is studied in this work mainly for providing an alternative circuit analysis method at post-processing period. Several different examples will be given to demonstrate the effectiveness of these MOR techniques mentioned above.

的研究者們。目前為止，多數應用不同電路算法的射頻微波設計軟件都直接輸出來用以研究及解決這類問題。部分非常常用算法（Partial Element Equivalent Circuit, PEEC）就是其中之一。PEEC 可以輕而易舉地將微波電路電磁域中的物理設計（RF layout）轉化為電路領域中分離元件——電阻、電容及電感互聯組成的電路模型。雖然 PEEC 給射頻設計與研究帶來了新思路，但是 PEEC 產生的非常複雜的電路網絡都會很大影響它在物理更複雜、工作頻率更高的射頻設計中應用，因此必須從模型降階（Model Order Reduction, MOR）理論來使這兩類射頻電路模型包含 PEEC 的系統化應用。近年來 MOR 已成為射頻電路計算機輔助設計領域的熱門研究課題。

本真論文研究了數學模型降階（Mathematical MOR）與物理模型降階（Physical MOR）兩種化簡辦法。其中數學化簡辦法將原先原來的電路系統狀態空間的模型到一個非常小的狀態空間上去，而後者還能保持大部分原來的輸入輸出特性。物理化簡辦法則直接按照一定規則直接一箇箇刪去電路中的節點以達到化簡電路的目的。

本真論文的重點在於物理化簡 MOR 這類射頻射頻電路降階（Physical MOR）中射頻電路網絡。論文提出兩種不同的物理化簡辦法實現大規模射頻電路模型化簡。一方面，由於數學化簡得到的模型不能再轉化為電路模型，因此物理化簡在本真文中只被用來後期輔助研究 PEEC 電路。此外本文還給出一條射頻電路化簡的系統化流程。

## 摘要

日益提高的工作頻率使得射頻設計中的寄生參數效應越來越嚴重地困擾著現今的研究者們。目前為止，十數個應用不同電磁算法的射頻輔助設計軟件相繼被開發出來用以研究及解決這類問題，部分元等效電路算法（Partial Element Equivalent Circuit, PEEC）就是其中之一。PEEC 可以輕而易舉地將無源電磁場領域中的佈局設計（RF layout）轉化為電路領域中分離元件——電阻、電容及電感互聯表示的電路模型。雖然 PEEC 給射頻設計與研究帶來了新思路，但是 PEEC 產生的非常複雜的電路網絡卻會極大影響它在佈局更複雜、工作頻率更高的射頻設計中應用，因而必須使用模型降階（Model Order Reduction, MOR）理論來化簡所得的電路模型以便 PEEC 的更廣泛應用。近年來 MOR 已成為射頻電路計算機輔助設計領域的熱門研究課題。

本篇論文研究了數學模型降階（Mathematical MOR）與物理模型降階（Physical MOR）兩類化簡辦法。其中數學化簡辦法將原先龐大的電路系統狀態空間投射到另一個非常小的狀態空間上去，而後者還能保持大部分前者的輸入輸出特性；物理化簡辦法則是按照一定規則直接一個個消去電路中的節點以達到化簡電路的目的。

本篇論文的重點在於物理化簡 PEEC 從無耗有源射頻佈局（RF passive design）中產生的電路網絡。論文提出兩種不同的物理化簡辦法實現大幅縮小電路規模的目的。另一方面，由於數學化簡得到的模型不能再轉化為電路網絡結構，因而數學化簡在本文中只被用來後期輔助研究 PEEC 電路。此外論文將給出一些例子實證這些化簡辦法的成果與效率。

## Acknowledgements

I would like to express my sincere thanks to my supervisor Professor Ke-Li Wu for his encouragement and precious advice all the way along my working on electromagnetics. His comprehensive knowledge and unique insight have greatly inspired me to pursue even higher goals.

Special thanks to Dr. Wang Jie for the invaluable discussions and suggestions. Without his exploratory work, this thesis can never be finished.

I would also like to thank my colleagues and my friends: Miss Ding Yan, Mr. Wei Dacheng, Mr. Meng Wei and Miss Hu Mengna for idea exchanges and helpful talks.

I can never forget my parents' consistent support on my life and my study.

*To my Beloved Parents:*    **HU Wei**  
   **LI Yulian**



# Table of Contents

<b>Author's Declaration .....</b>	<b>ii</b>
<b>Abstract.....</b>	<b>iii</b>
<b>Acknowledgements .....</b>	<b>vi</b>
<b>Table of Contents .....</b>	<b>viii</b>
<b>List of Figures.....</b>	<b>xi</b>
<b>List of Tables .....</b>	<b>xiv</b>
<b>Chapter 1 Introduction.....</b>	<b>1</b>
1.1 Background .....	1
1.2 Overview of This Work.....	2
1.3 Original Contributions in the Thesis .....	3
1.4 Thesis Organization.....	4
<b>Chapter 2 PEEC Modeling Background .....</b>	<b>5</b>
2.1 Introduction .....	5
2.2 PEEC Principles .....	6
2.3 Meshing Scheme .....	10
2.4 Formulae for Calculating the Partial Elements .....	12
2.4.1 Partial Inductance .....	12
2.4.2 Partial Capacitance .....	14
2.5 PEEC Application Example .....	15
2.6 Summary .....	17
References .....	18
<b>Chapter 3 Mathematical Model Order Reduction.....</b>	<b>20</b>

3.1 Introduction .....	20
3.2 Modified Nodal Analysis .....	21
3.2.1 Standard Nodal Analysis Method Review.....	22
3.2.2 General Theory of Modified Nodal Analysis .....	23
3.2.3 Calculate the System Poles Using MNA .....	27
3.2.4 Examples and Comparisons.....	28
3.3 Krylov Subspace MOR Method.....	30
3.4 Examples of Krylov Subspace MOR .....	32
3.5 Summary .....	34
References .....	35
<b>Chapter 4 Physical Model Order Reduction .....</b>	<b>38</b>
4.1 Introduction .....	38
4.2 Gaussian Elimination Method.....	39
4.3 A Lossy PEEC Circuit Model .....	44
4.3.1 Loss with Capacitance .....	44
4.3.2 Loss with Inductance .....	46
4.4 Conversion of Mutual Inductive Couplings .....	47
4.5 Model Order Reduction Schemes.....	50
4.5.1 Taylor Expansion Based MOR Scheme (Type I).....	51
4.5.2 Derived Complex-valued MOR Scheme (Type II) .....	65
4.6 Summary .....	88
References .....	88
<b>Chapter 5 Concluding Remarks .....</b>	<b>92</b>

5.1 Conclusion.....	92
5.2 Future Improvement.....	93
<b>Author's Publication.....</b>	<b>95</b>

## List of Figures

Figure 2.1 Typical stratified LTCC structure.....	6
Figure 2.2 Discretized MPIE. ....	9
Figure 2.3 Microstrip and its meshes. ....	11
Figure 2.4 Meshes and the equivalent circuit model. ....	12
Figure 2.5 Two parallel rectangular inductive meshes .....	13
Figure 2.6 LTCC low-pass filter. ....	15
Figure 2.7 Netlist obtained from PEEC modeling. ....	16
Figure 2.8 S-parameters comparison between EM model and PEEC model.....	17
Figure 3.1 Example two-port network. ....	24
Figure 3.2 Planar spiral inductor.....	29
Figure 3.3 S-parameters comparison between the original model and the mathematical MOR model of a LTCC low-pass filter. ....	32
Figure 3.4 A typical LTCC band-stop filter.....	33
Figure 3.5 S-parameters comparison between the original model and the mathematical MOR model of a LTCC band-pass filter. ....	34
Figure 4.1 A simple four-node circuit network.....	40
Figure 4.2 Y- $\Delta$ transformation.....	43
Figure 4.3 Capacitance and its loss.....	45
Figure 4.4 Inductance and its loss.....	46
Figure 4.5 A pair of coupled inductances. ....	47
Figure 4.6 The equivalent non-coupled inductance network.....	49
Figure 4.7 Lossy equivalent non-coupled inductances. ....	50

Figure 4.8 Basic electrical components for the lossy circuit. ....	52
Figure 4.9 Lossy inductances connecting to node x. ....	53
Figure 4.10 Combination of lossy inductances. ....	54
Figure 4.11 PA output matching network. ....	60
Figure 4.12 S-parameters magnitude (a) and phase (b) of the EM model, PEEC model and Type I MOR reduced model of PA output network. ....	61
Figure 4.13 A multi-layer high-pass filter. ....	62
Figure 4.14 S-parameters comparison of the EM model, PEEC model and Type I MOR reduced model of a high-pass filter. ....	63
Figure 4.15 Equivalent circuit of $y_{mn}$ . ....	68
Figure 4.16 Simple illustration of equivalent inductance. ....	70
Figure 4.17 Vector representation of $\tilde{L}_i$ . ....	72
Figure 4.18 Inductance's change with the mesh shape. ....	74
Figure 4.19 Three-layered RF planar inductor. ....	75
Figure 4.20 Reduced circuit model for the RF planar inductor. ....	76
Figure 4.21 S-parameters magnitude (a) and phase (b) of the EM model, PEEC model and Type II MOR model of the RF planar inductor. ....	77
Figure 4.22 Quality factors of the EM model, PEEC model and Type II MOR model of the RF planar inductor. ....	78
Figure 4.23 Four-layered RF planar capacitor. ....	79
Figure 4.24 Reduced circuit model for the RF planar capacitor. ....	80
Figure 4.25 S-parameters magnitude (a) and phase (b) of the EM model, PEEC model and Type II MOR model of the RF planar capacitor. ....	81

Figure 4.26 Quality factors of the EM model, PEEC model and Type II MOR model of the RF planar capacitor. ....	82
Figure 4.27 Reduced circuit model for the RF high-pass filter. ....	83
Figure 4.28 S-parameters magnitude (a) and phase (b) of the EM model, PEEC model and Type II MOR model of RF high-pass filter.....	84
Figure 4.29 Five-layered RF band-pass filter. ....	85
Figure 4.30 Reduced circuit model for the RF band-pass filter.....	86
Figure 4.31 S-parameters comparison of the EM model, PEEC model and Type II MOR model of RF band-pass filter.....	87
Figure 4.32 In-band plot of the curves in Figure 4.31. ....	87

## List of Tables

Table 3.1 System poles. ....	29
Table 4.1 Type I MOR case summary. ....	65
Table 4.2 Components values for the reduced circuit of the RF planar inductor. ....	76
Table 4.3 System poles change for the RF planar inductor. ....	78
Table 4.4 Components values for the reduced circuit of the RF planar capacitor.....	80
Table 4.5 System poles change for the RF planar capacitor.....	82
Table 4.6 Components values for the reduced circuit of RF high-pass filter. ....	83
Table 4.7 Components values for the reduced circuit of RF band-pass filter.....	86

# Chapter 1

## INTRODUCTION

### 1.1 Background

As the RF/ Microwave chips have been designed more compact than ever before, along with the increase of the speed of the signal traveling down the PCB boards and IC chips, the parasitic effect is inevitable. Typical example lies in the design of wireless communication products, where the demanding market requirement on the performance and functionality has created critical need to reduce the size and cost of the passive components, which in turn has impelled the development of highly integrated packaging technologies, e.g., system on package (SOP) such as low temperature co-fired ceramic (LTCC). However, as the operating frequency is still fast going up, existing electronic design automatic tools can awkwardly meet the needs in the design flow. One major limit is the lack of the ability to systematically transform layout patterns into reasonable lumped circuit models corresponding only to physical features of the layout rather than curve fitting to some predefined generalized circuit model. In short of this ability, the lack of the physical insight behind the circuits can make the designer hardly diagnose or adjust their design promptly. Therefore a methodology to extract the circuit model from the layout and efficiently diagnose the resultant circuit is highly desirable.

Several techniques such as Partial Element Equivalent Circuit (PEEC) method is thus developed to recover equivalent circuit model from electromagnetic (EM) model. PEEC is one of the integral equation based methods. Classic PEEC solver utilizes Green's function ana-



lytically or numerically to convert physical layout into passive *RLC* circuit networks, including mutual couplings. Once the circuit model is obtained, any circuit solver, such as SPICE, can manage the rest of the job. Unfortunately, the number of nodes and components in the resultant circuit are dependent on the complexity of the original layout. Hence, the increasingly complicated RF circuit layout under RF or even microwave frequency can bring along an equivalent network in excessive large scale, which is obviously time-consuming to deal with. Thus what the researchers are searching for nowadays are measures that can significantly reduce the model orders for accelerating the analysis of the circuit network.

## 1.2 Overview of This Work

There are three parts composed in this thesis. The first part is about the PEEC algorithm, from which the other two parts are evolved. The second and third parts are about two different paths to a final simplified model. Though, each of them has its individual cons and pros, both of them can be used to for Model Order Reduction (MOR) for RF circuits design and diagnosis.

The circuit model to which the reduction scheme is going to apply is a crucial part in the whole reduction process. Only performed upon the foundation laid by reasonable layout-to-circuit transformation, the whole reducing and analyzing procedures can be accomplished. Therefore, understanding PEEC algorithm would be of very important for building a rigorous and efficient MOR scheme.

The PEEC algorithm employed is mainly based on the works of previous researchers in the research group in CUHK. After several years' continuous effort, the PEEC algorithm based circuit extractor and solver can handle not only the regular shaped circuit layout, but also the

semi-irregular shaped geometries such as annulus and the mix of those shapes at interconnections. The current version of PEEC solver works under quasi-static approximation, for the circuit size under consideration is usually much smaller than the operating wavelength, thus with this approximation real-valued circuit components can be extracted immediately. In the near future, derived physically expressive circuit model based on the full-wave PEEC modeling with complex-valued circuit components will be introduced.

This thesis mainly focuses on model order reduction (MOR) schemes to PEEC circuits. Two main categories of reduction schemes, namely the mathematics-based MOR and physics-based MOR are discussed in detail. The principle of the former one was first introduced in control theory, but is gaining popularities recently, for it can greatly simplify the macromodel of the circuit network in a very short time period with just one single matrices transformation. What's more, the obtained response curves of the reduced system can have little difference from the original circuit model. On the contrary, the physical MOR scheme can only eliminate one circuit node at each reduction step, thus it might cost a slightly longer time to finish the whole reduction. However, this physics-based scheme strictly follows the electronic property of the whole circuit topology, which makes the resultant reduced macromodel physically meaningful. The resultant circuit is realizable by all available passive components, i.e., resistors, capacitors and inductors, which were also the constituents of original lumped circuit network from PEEC modeling.

### **1.3 Original Contributions in the Thesis**

The main contributions of this work include

- (1). It has incorporated the mathematics-based MOR scheme with a PEEC solver, which has substantially improved the efficiency of the PEEC solver. Besides, with this MOR's application, the critical system poles extraction process has been stabilized.
- (2). A physics-based MOR scheme dealing with lossy multi-layered RF circuits is developed. The mathematic condition that guarantees the passivity of the MOR scheme is given.
- (3). A mathematic justification of the physical meaning of the resultant reduced circuit model at each MOR step is provided by analyzing the eigenvalues (system poles) of each intermediate circuit model.

## 1.4 Thesis Organization

The remainder of this thesis is organized as follows. Basic knowledge of PEEC will be introduced in chapter 2, where the deduction process for the expression used in calculating the partial inductances and partial capacitances will be presented. In chapter 3, details on mathematics-based reduction schemes and its application on boosting the efficiency of the post-analysis will be given. Chapter 4 talks about two different physics-based MORs, besides, special attention will be paid to the lossy PEEC model. In chapter 5, some concluding remarks and the future plans are given.

## Chapter 2

# PEEC MODELING BACKGROUND

### 2.1 Introduction

Before performing MOR, the target circuit must be prepared. Although there are various ways to generate the circuit, a widely applied technique, PEEC, is so far the most efficient and practical modeling method. PEEC can translate layout design into lumped circuit model corresponding to layout meshes.

The advantage of analyzing multi-layered layout design in circuit domain is obvious. Traditional EM solvers are concentrating on numerically discretizing and solving the integral or differential Maxwell equations so as to give accurate simulation data. However, it might take hours or even longer time for simulating a medium scale multi-layered design. Moreover, curves obtained from EM simulation still lack overall vision on the whole system's performance, which is quite a weakness for the diagnosis and re-design process. On the contrary, if the whole layout can be expressed in circuit domain according to its physical behavior, then this will tremendously benefit the design flow. Not only can the obtained circuit model be fed into any SPICE-like solver to find out frequency domain response or time domain response, but the generated topology is also a treasure to RF designers. Because unlike any predefined inflexible models, PEEC circuit has embodied local property of the original layout design, which can assist RF designer to grasp the key directions when modifying their rough drafts.

The concept of PEEC is first brought up by Albert E. Ruehli in 1974[1]. It is based on discretization of the electric field integral equation (EFIE) problem, where EFIE can be inter-

preted in terms of the capacitive [2] and inductive [3] interaction between the elemental charges and currents. After more than two decades' development, this method is mature and competitive both in academic realm and industrial application realm. The driving force here in the Chinese University of Hong Kong for advancing PEEC technique development is PEEC's practical use in LTCC passive devices design. The stratified LTCC structure, such as that shown in Figure 2.1, is the optimal target for PEEC method. LTCC chip's size is usually less than one tenths of the wavelength of the RF signal operating on it, thus quasi-static approximation is applicable to PEEC method.

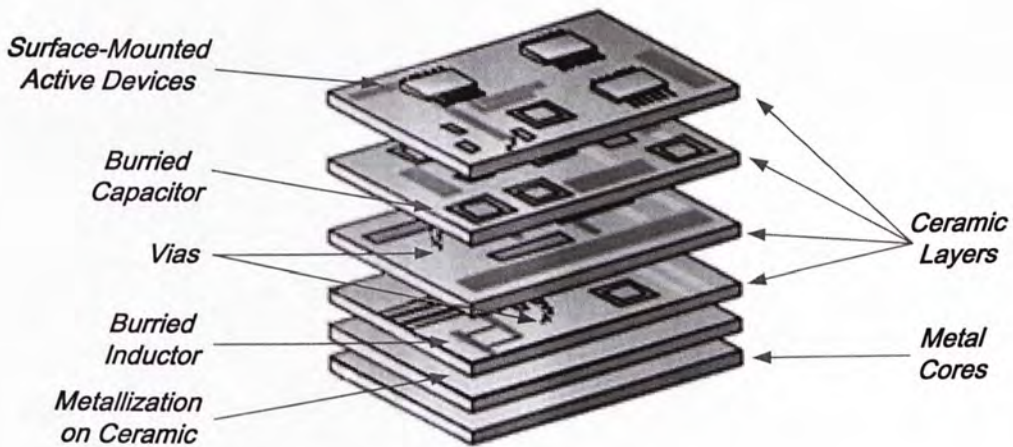


Figure 2.1 Typical stratified LTCC structure.

A brief introduction to PEEC fundamentals are presented in the rest of this chapter serving as the pre-knowledge of MOR analysis.

## 2.2 PEEC Principles

PEEC theory starts from electric field, where the field at any arbitrary point in the region of interest can be expressed as:

$$\mathbf{E}(\mathbf{r}, t) = \frac{\mathbf{J}(\mathbf{r}, t)}{\sigma}, \quad (2.1)$$

$$\mathbf{E}(\mathbf{r}, t) = \mathbf{E}^i(\mathbf{r}, t) + \mathbf{E}^s(\mathbf{r}, t). \quad (2.2)$$

Equation (2.1) is the exact Ohm's law in point form, where  $\mathbf{J}$  is current density,  $\sigma$  is conductivity. In equation (2.2),  $\mathbf{E}^i(\mathbf{r}, t)$  is the incident field, and  $\mathbf{E}^s(\mathbf{r}, t)$  is the scattering field.

As is known,  $\mathbf{E}^s(\mathbf{r}, t)$  can be expressed more specifically as:

$$\mathbf{E}^s(\mathbf{r}, t) = -\nabla\Phi(\mathbf{r}, t) - \frac{\partial\mathbf{A}(\mathbf{r}, t)}{\partial t}, \quad (2.3)$$

where  $\mathbf{A}(\mathbf{r}, t)$  is vector magnetic potential, and  $\Phi(\mathbf{r}, t)$  is electric potential. Then if a total  $K$  conducting bodies exist in this system:

$$\mathbf{A}(\mathbf{r}, t) = \sum_{k=1}^K \frac{\mu}{4\pi} \int_{v_k} G(\mathbf{r}, \mathbf{r}') \mathbf{J}(\mathbf{r}', t') dv'_k \quad (2.4)$$

$$\Phi(\mathbf{r}, t) = \sum_{k=1}^K \frac{1}{4\pi\epsilon} \int_{v_k} G(\mathbf{r}, \mathbf{r}') q(\mathbf{r}', t') dv'_k, \quad (2.5)$$

where  $G(\mathbf{r}, \mathbf{r}')$  is the Green's function in this region,  $\mathbf{J}(\mathbf{r}', t')$  is the current density in the conducting bodies, and  $q(\mathbf{r}', t')$  is the charge density on the surface of the conducting bodies. Variables with "'' indicate the source point, while in absence of "'' indicate the observing point.

Further divide this multi-conductor system into a total  $N$  small volume cells, and then mathematically, current density  $\mathbf{J}$  at the observing point can be expanded like

$$\mathbf{J}(\mathbf{r}, t) = \sum_{n=1}^N \mathbf{J}_n(\mathbf{r}, t) P_n(\mathbf{r}), \quad (2.6)$$

where

$$P_n(\mathbf{r}) = \begin{cases} 1 & \mathbf{r} \in n_{th} \text{ volume cell} \\ 0 & \mathbf{r} \in \text{other volume cells} \end{cases} \quad (2.7)$$

$P_n(\mathbf{r}, t)$  is just the pulse function which helps denote the position information of the volume cell.

Similarly, as the charge is always located on the surface of conducting bodies, we can also discretize the system into  $M$  surface cells, and then the charge density  $q$  can be expanded like

$$q(\mathbf{r}, t) = \sum_{m=1}^M q_m(\mathbf{r}, t) T_m(\mathbf{r}), \quad (2.8)$$

where

$$T_m(\mathbf{r}) = \begin{cases} 1 & \mathbf{r} \in m_{th} \text{ surface cell} \\ 0 & \mathbf{r} \in \text{other surface cells} \end{cases} \quad (2.9)$$

$T_m(\mathbf{r})$  is also a pulse function which denotes the position information of the surface cell.

Since the system can be divided into infinitesimal cells, we assume the current density and charge density on individual cell is constant.

After the above discretization process, incident field  $\mathbf{E}^i(\mathbf{r}, t)$  in equation (2.2) turns out to be

$$\begin{aligned} \mathbf{E}^i(\mathbf{r}, t) = & \frac{\mathbf{J}(\mathbf{r}, t)}{\sigma} + \sum_{k=1}^K \sum_{n=1}^N \frac{\mu}{4\pi} \left[ \int_{v_{nk}} G(\mathbf{r}, \mathbf{r}') dv'_{nk} \right] \frac{\partial \mathbf{J}_{nk}(t')}{\partial t} \\ & + \sum_{k=1}^K \sum_{m=1}^M \frac{1}{4\pi\epsilon} \nabla \left[ q_{mk}(t') \int_{s_{mk}} G(\mathbf{r}, \mathbf{r}') ds'_{mk} \right]. \end{aligned} \quad (2.10)$$

Equation (2.10) is the well-known mixed potential integrated equation (MPIE) in discretized form. Since the aim of the PEEC is to extract the circuit components from the EM domain, we apply Galerkin matching procedure [4][5] on both sides of equation (2.10). Taking advantage of the fact that there is no incident field in this region, equation (2.10) is finally converted into a voltage summation form like:

$$0 = V_R + V_L + V_C. \quad (2.11)$$

$V_R$ ,  $V_L$  and  $V_C$  in equation (2.11) represent the resistive, inductive and capacitive voltage drops over the conducting bodies respectively. They are illustrated in Figure 2.2. Detailed information on Galerkin matching method and the deduction procedure for  $V_R$ ,  $V_L$  and  $V_C$  can be found in [5].

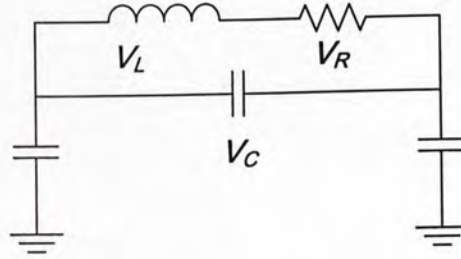


Figure 2.2 Discretized MPIE.

In Cartesian coordinates, the vector variable  $\mathbf{J}$  and Laplacian operator  $\nabla$  all have components in  $x$ ,  $y$  and  $z$  directions, therefore the voltage values in equation (2.11) are also have three components. We list the  $x$  direction component below:

$$V_{Rx} = \frac{1}{a_l \sigma} \int_{v_l} J_x(\mathbf{r}, t) dv_l; \quad (2.12)$$

$$V_{Lx} = \sum_{k=1}^K \sum_{n=1}^N \frac{\mu}{4\pi a_l} \left[ \int_{v_l} \int_{v_{nk}} G(\mathbf{r}, \mathbf{r}') dv'_{nk} dv_l \right] \frac{\partial J_{nk}^x(t')}{\partial t}; \quad (2.13)$$



$$V_{Cx} = \sum_{k=1}^K \sum_{m=1}^M \frac{1}{4\pi\epsilon a_l} \int_{v_l} \frac{\partial}{\partial x} \left[ q_{mk}(t') \int_{s_{mk}} G(\mathbf{r}, \mathbf{r}') ds'_{mk} \right] dv_l, \quad (2.14)$$

where subscript  $l$ ,  $nk$  and  $mk$  indicate different cells, and  $a_l$  is cross area of the volume cell  $v_l$ .

Since Green's functions for stratified structures are well established, in the following sections we can use the voltages equations above to calculate values of inductances and capacitances, which constitute the PEEC circuit model. Our original intention to apply PEEC modeling is to deal with LTCC packages, whose loss effect is considerably low. Therefore, lossy elements are excluded in current version of our PEEC algorithm. Furthermore, in section 2.5, the response curves generated by PEEC algorithm and those obtained from commercial full-wave EM solvers are compared.

We will extend PEEC algorithm in chapter 4 in order to handle other EM packages, such as high-speed PCBs, where lossy effect must be considered.

### 2.3 Meshing Scheme

The way to partition conducting bodies directly influences the accuracy of PEEC circuit. In order to be consistent with basic PEEC theory, the meshes used in computation are categorized into two groups, one is called inductive mesh, which is used equation (2.13), the other is called capacitive mesh, which is used in equation (2.14). Basically the meshes are in regular shape, i.e. rectangles. Though in some design cases, circular, annular or their mixed shapes are also adopted, we all managed to have them appropriately treated [6]-[8].

The size of mesh is related to the highest operating frequency, whose wavelength is  $\lambda_{\min}$ . Usually the shape of mesh is chosen to be smaller than one twentieth of  $\lambda_{\min}$  to ensure an acceptable error rate and a relatively fast simulation speed.

A typical illustration of the mesh scheme is shown below:

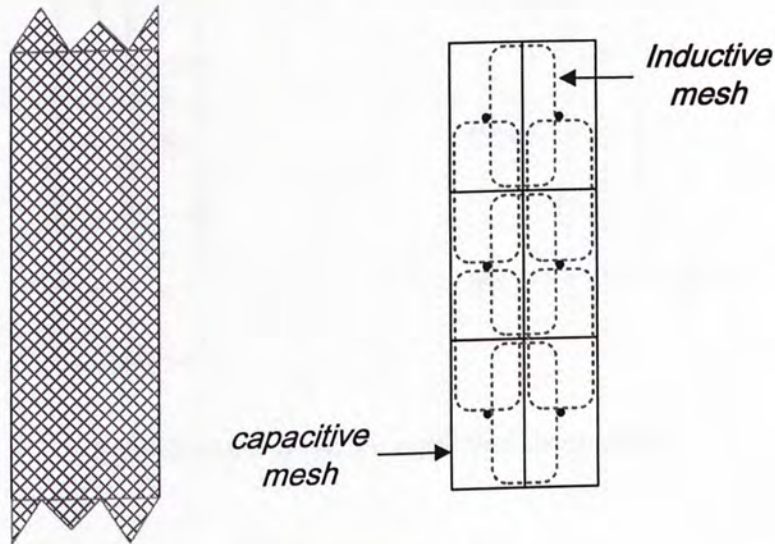


Figure 2.3 Microstrip and its meshes.

On the left side of Figure 2.3 is part of a common microstrip line (the thickness is ignored). On the right side is the same microstrip but with two types of meshes on it: The black solid rectangles with nodes in their centers represent capacitive meshes, while the red dotted rectangles represent inductive meshes, which are usually one half size offset from their neighbor capacitive meshes. If the operating frequency has increased, meshes will be created smaller and denser accordingly.

The resultant circuit model from the meshes above is shown in Figure 2.4, where mutual capacitances and mutual inductances are not plotted for letting the figure clear. In fact, mutual elements play an important role in PEEC modeling.

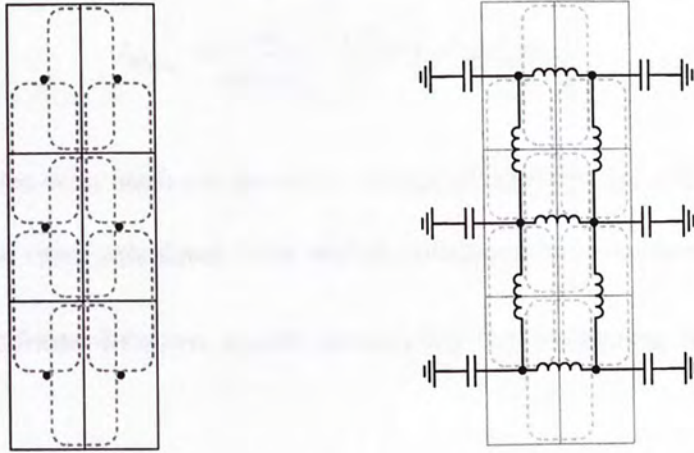


Figure 2.4 Meshes and the equivalent circuit model.

## 2.4 Formulae for Calculating the Partial Elements

This section introduces analytical ways to calculate capacitances and inductances, such as those shown in Figure 2.4.

### 2.4.1 Partial Inductance

The formula for partial inductance is derived from equation (2.13). Replacing current density  $J_{nk}$  with current  $I$  divided by cross area  $a_{nk}$ , equation (2.13) becomes

$$V_{Lx} = \sum_{k=1}^K \sum_{n=1}^N \frac{\mu}{4\pi a_l a_{nk}} \left[ \int_{v_l} \int_{v_{nk}} G(\mathbf{r}, \mathbf{r}') dv'_{nk} dv_l \right] \frac{\partial I_{nk}^x(t')}{\partial t}. \quad (2.15)$$

Comparing equation (2.15) with inductance's definition equation below:

$$V_L = L \frac{\partial I_L}{\partial t}, \quad (2.16)$$

we can find out an equivalent partial inductance  $L_{p_{l,nk}}$  between the observing mesh  $l$  and the source mesh  $nk$ :

$$L_{P_{l,nk}} = \frac{\mu}{4\pi a_l a_{nk}} \left[ \int_{v_l} \int_{v_{nk}} G(\mathbf{r}, \mathbf{r}') dv'_{nk} dv_l \right]. \quad (2.17)$$

If mesh  $l$  coincides with mesh  $nk$ , the value calculated above is the self-inductance of this mesh; otherwise the value calculated is the mutual inductance between those two meshes.

For a uniform infinite dielectric region surrounding the conducting bodies, the Green's function is

$$G(\mathbf{r}, \mathbf{r}') = \frac{1}{|\mathbf{r} - \mathbf{r}'|}. \quad (2.18)$$

Then the inductance between two thin rectangular inductive meshes in parallel (shown in Figure 2.5) can be analytically calculated out by substituting (2.18) into equation (2.17).

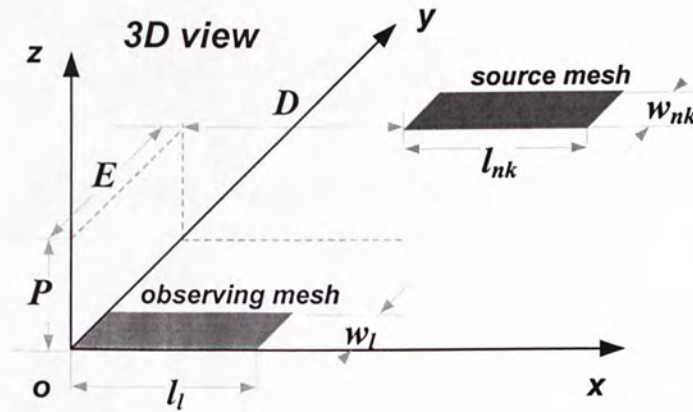


Figure 2.5 Two parallel rectangular inductive meshes.

After integration,  $L_{P_{l,nk}}$  becomes: [6]

$$L_{P_{l,nk}} = \frac{\mu}{4\pi w_l w_{nk}} \sum_{i=1}^4 \sum_{j=1}^4 (-1)^{i+j} \left[ \frac{y_j^2 - P^2}{2} x_i \ln(x_i + \rho_{ij}) + \frac{x_j^2 - P^2}{2} y_i \ln(y_i + \rho_{ij}) \right. \\ \left. - \frac{\rho_{ij}}{6} (x_i^2 + y_j^2 - 2P^2) - x_i y_j P \tan^{-1} \frac{x_i y_j}{\rho_{ij} P} \right], \quad (2.19)$$

where

$$\begin{aligned}
 \rho_{ij} &= \sqrt{x_i^2 + y_j^2 + P^2}, \\
 x_1 &= D - l_l, & x_2 &= D + l_{nk} - l_l; & y_1 &= E - w_l, & y_2 &= E + w_{nk} - w_l; \\
 x_3 &= D + l_{nk}, & x_4 &= D; & y_3 &= E + l_{nk}, & y_4 &= E.
 \end{aligned} \tag{2.20}$$

For different regional situations, Green's function varies. Besides if irregular shaped meshes are adopted, numerical integration may need to extract the inductances [6].

### 2.4.2 Partial Capacitance

Expression for partial capacitance is derived from equation (2.14). Replacing the partial derivative appeared in (2.14) with central finite difference approximation [5][6], equation (2.14) becomes

$$V_{Cx} = \sum_{k=1}^K \sum_{m=1}^M \frac{Q_{mk}(t')}{4\pi\epsilon S_{mk}} \left[ \int_{s_{mk}} G(\mathbf{r}_l^+, \mathbf{r}') ds'_{mk} - \int_{s_{mk}} G(\mathbf{r}_l^-, \mathbf{r}') ds'_{mk} \right], \tag{2.21}$$

in which  $Q_{mk}$  stands for the total charge on mesh  $mk$ ,  $S_{mk}$  is the area of this mesh, and

$$\mathbf{r}_l^+ = \left( x_l + \frac{\Delta x_l}{2}, y_l, z_l \right), \quad \mathbf{r}_l^- = \left( x_l - \frac{\Delta x_l}{2}, y_l, z_l \right). \tag{2.22}$$

Equation (2.22) explains why capacitive meshes are chosen to be one half sizes offsetting from inductive meshes, or vice versa.

Comparing equation (2.21) with the equation (2.23) that describes the relation between voltage and charge over a capacitor,

$$V_C = \frac{Q_C}{C}, \tag{2.23}$$

the reciprocal of the capacitance between the observing mesh  $l$  and the source mesh  $mk$ ,  $pp_{l,mk}$  can be found out: [2][5]

$$pp_{l,mk} = \frac{1}{4\pi\epsilon S_l S_{mk}} \left[ \int_{S_l} \int_{S_{mk}} G(\mathbf{r}_l^+, \mathbf{r}') ds'_{mk} ds_l \right]. \quad (2.24)$$

Since the integrand in (2.24) is the same as that in (2.17), a very similar result can be analytically acquired. Inverting matrix  $PP$ , whose individual entry is  $pp_{l,mk}$ , another matrix  $CS$  for mutual capacitances is obtained, i.e.  $CS = PP^{-1}$ . From  $CS$ , self-capacitances and mutual capacitances can be easily computed [6].

## 2.5 PEEC Application Example

A typical LTCC low-pass filter design is demonstrated in Figure 2.6.

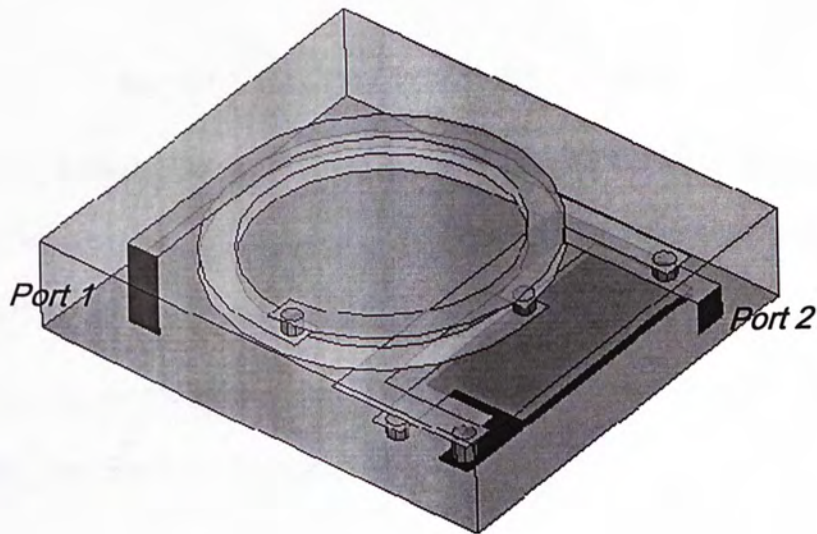


Figure 2.6 LTCC low-pass filter.

The working frequency ranges from 0.5GHz to 5GHz. The dimension of the dielectric box that encloses the whole design is 1.96mm × 2.25mm × 0.437mm, and the width for all strips is 0.15mm. A total 62 capacitive meshes are created. After PEEC process we can get a SPICE-like netlist for the equivalent circuit:

```
.ELEMENTS
CAP 1 62 C = 0.1267883p
CAP 2 62 C = 0.1211353p
CAP 3 62 C = 0.1249637p
CAP 4 62 C = 0.1567388p
CAP 5 62 C = 0.0131962p
CAP 6 62 C = 0.0091213p
.
.
.
MUL 1 2 2 3 L1 = 0.0697714n L2 = 0.0697714n M = 0.0043174n
MUL 1 2 5 6 L1 = 0.0697714n L2 = 0.0992511n M = 0.0432078n
MUL 1 2 6 7 L1 = 0.0697714n L2 = 0.0992511n M = 0.0054034n
MUL 1 2 9 34 L1 = 0.0697714n L2 = 0.0834969n M = 0.0050785n
MUL 1 2 24 25 L1 = 0.0697714n L2 = 0.0563982n M = 0.0094187n
MUL 1 2 27 28 L1 = 0.0697714n L2 = 0.0828234n M = 0.0118060n
MUL 1 2 28 29 L1 = 0.0697714n L2 = 0.0828234n M = 0.0024678n
MUL 1 2 34 35 L1 = 0.0697714n L2 = 0.1330496n M = 0.0068629n
.
.
.
```

Figure 2.7 Netlist obtained from PEEC modeling.

*CAP* and *MUL* in Figure 2.7 describe the capacitances and mutual inductances extracted, respectively. Since there are 190 capacitors, 70 inductors with 306 mutual couplings, only a small portion of the netlist is shown in Figure 2.7.

The S-parameter curves obtained both from a commercial EM solver (Ansoft HFSS v.8.0, same hereinafter) and the PEEC algorithm are compared below:

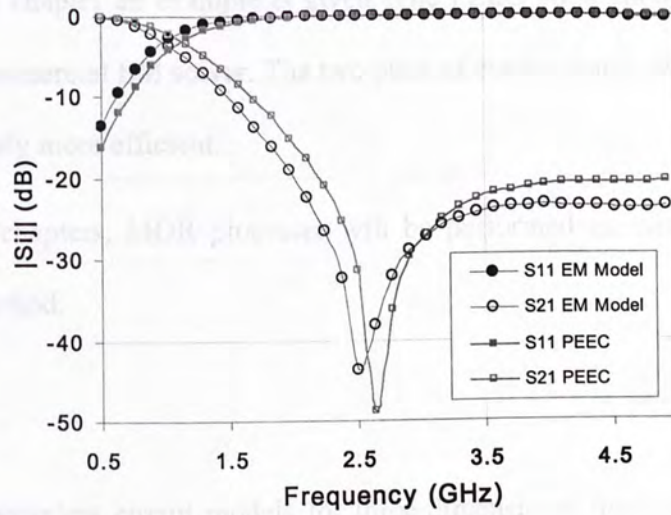


Figure 2.8 S-parameters comparison between EM model and PEEC model.

The two pairs of curves agree with each other very well, but it only cost the PEEC solver less than 10 seconds to obtain the netlist and another 3 seconds to compute the S-parameters from the netlist, while the commercial EM solver spend more than 2 minutes to achieve a similar result. The efficiency of PEEC is quite clear.

## 2.6 Summary

In this chapter, a brief introduction to the basic knowledge of PEEC algorithm is given.

PEEC method is based on mixed potential integration equation (MPIE), which is evolved from basic EM equations. After performing Galerkin matching method to the discretized MPIE, the resultant equations are self-evident for extracting the lumped components we are after.



In the end of the chapter an example is given. The PEEC simulation result is compared with that from a commercial EM solver. The two pairs of curves match well; however, PEEC modeling is obviously more efficient.

In the next two chapters, MOR processes will be performed on circuits obtained from PEEC modeling method.

## References

- [1] E. Ruehli, "Equivalent circuit models for three-dimensional multi-conductor systems," *IEEE Trans. Microwave Theory Tech.*, vol. 22, no. 3, pp. 216-221, March 1974.
- [2] E. Ruehli and P. A. Brennan, "Efficient capacitance calculations for three-dimensional multi-conductor systems," *IEEE Trans. Microwave Theory Tech.*, vol. 21, no. 2, pp. 76-82, Feb. 1973.
- [3] E. Ruehli, "Inductance calculations in a complex integrated circuit environment," *IBM J. Res. Develop.*, vol. 16, pp. 470-481, Sept. 1972.
- [4] R. F. Harrington, "*Field Computation by Moment Methods*," New York: Macmillan, 1993, ch.1.
- [5] L. K. Yeung, "PEEC Modeling of LTCC Embedded RF Passive Devices," Mphil. thesis, Chinese University of Hong Kong, 2002, ch. 2.
- [6] M. Hu, "Enhanced PEEC Electromagnetic Modeling for RF/Microwave Multi-layer Circuits," Mphil. thesis, Chinese University of Hong Kong, 2004, ch. 2.
- [7] D. K. Reitan, "Accurate determination of the capacitance of rectangular parallel-plate capacitors," *J. Appl. Phys.*, vol. 30, pp. 172-176, Feb. 1959.

- [8] C. Hoer and C. Love, "Exact inductance equations for rectangular conductors with applications to more complicated geometries," *J. Res. Natl. Bur. Stand. C*, vol. 69, no. 2, pp. 127-137, Apr.-June 1965.

### 3.1 Introduction

The principle of PEEC algorithm is given in chapter 2. As we can see, the higher the operating frequency, the denser the meshes will be, hence more complex environment will be required to model the parasitic effects in more detail. Even though some commercial circuit solvers can deal with large network with tens of thousands of nodes, with the fast increasing density of the resultant circuit model, only updating the circuit solver algorithm can be insufficient with the needs of rapid simulation expected in RF design industries. Consequently, researchers are now focusing on techniques to reduce the macro-model size by decomposing it into a macro-model and a circuit solver. The macro-model refers to those mathematical models at circuit-level, such as the well-known modified nodal analysis (MNA) model.

Generally speaking, MOR can be categorized into two groups: model-based MOR, and the mathematics-based MOR. The model-based MOR is based on the original circuit model to represent the original over-sized circuit network. The mathematics-based MOR concentrates on gradually simplifying the circuit model by removing the nodes of the circuit's non-unique attributes. The first group of MOR techniques transform the whole reduction process into a mathematical model, which is well described and tested in state-space. With state-space method, the reduction of the circuit model is in linear algebraic form, the original state-space is transformed into a reduced state-space.

## Chapter 3

# MATHEMATICAL MODEL ORDER REDUCTION

### 3.1 Introduction

The principle of PEEC algorithm is given in chapter 2. As we can see, the higher the working frequency, the denser the meshes will be, hence more lumped components will be extracted to model the parasitic effects in more detail. Even though some optimized circuit solvers can deal with large network with tens of thousands of nodes, with the fast increasing density of the resultant circuit model, only updating the circuit solver algorithm can no longer catch up with the needs of rapid simulation expected in RF design industries. Consequently, researchers are now focusing on techniques to reduce the macromodel orders of a system before solving it by a circuit solver. The macromodel refers to those matrices-expressed models on system level, such as the well-known modified nodal analysis (MNA) matrices.

Generally speaking, MOR can be categorized into two groups: one is called the physics-based MOR, and the other is the mathematics-based MOR. They both aim to achieve a reduced model to represent the original over-sized circuit network. However, the former method concentrates on gradually simplifying the circuit complexity. During the MOR, coherence of the circuit's electronic attributes is the first concern. Whereas the latter method turns the whole reduction process into a mathematical venture and a circuit network is described and treated in state-space. With space projection method and maturely developed iterative algorithms in linear algebras, the original state-space is replaced by a small-sized new

state-space. Usually the only link between those two state-spaces is their nearly identical input-output transfer function. In this chapter we focus on the mathematics-base MOR.

The mathematics-based MOR problem is originated from systems control theory research, where how to reduce the complexity of dynamical systems yet preserving (to the possible extent) their input-output behaviors were studied [1]. The first work on MOR in circuit area is asymptotic waveform evaluation (AWE) [2], which is based on Padé approximation method. After AWE, several other Padé-related MOR methods are derived, such as Padé via Lanczos (PVL) [3], matrix PVL (MPVL, for multi-input multi-output (MIMO) systems) [4]. More recently, Krylov-subspace method, especially its derivative, Arnoldi process [5]-[7], has drawn researchers' attentions.

Even though the theory of mathematical MOR is relatively mature, its applications are still limited. In [6][7] and many other publications, only simple transmission line circuit models or networks from predefined cascaded prototypes are tested. Thus in this chapter, we try to incorporate mathematical MOR with our PEEC model to achieve even faster simulation model for solving those complicated RF passive circuits.

The rest of this chapter is organized as follows. First the nodal analysis methods, both standard and modified, are introduced. Then, the procedure of Krylov subspace based Arnoldi reduction process is presented. Numerical examples are given to show the effectiveness and limitation, which is followed by a summary.

### **3.2 Modified Nodal Analysis**

Modified Nodal Analysis method is used for computer programming to systematically solve a circuit problem. Even though this method may result in larger scale system equations than

other methods, it has facilitated the computer algorithm implementation. The MNA method can be applied to a PEEC model to solve for the frequency domain response directly. We also use it as the foundation for mathematical MOR.

Prior to introducing the theory of MNA, standard nodal analysis (SNA) will be briefly discussed. After presenting the principle of MNA, we will demonstrate how to take advantage of it for calculating the system poles.

### 3.2.1 Standard Nodal Analysis Method Review

The SNA method can be easily understood by solving a small scale circuit. The basic procedure for an  $n$ -node network with  $m$  voltage sources is given below: [8]

- (1). Choosing a node as the datum node (ground node);
- (2). Numbering the rest of the  $n-1$  nodes;
- (3). Applying the Kirchhoff current law to all the nodes that do not connect with a voltage source; and
- (4). Solving the remaining  $n-1-m$  unknown voltages at nodes.

We do not need to find out the voltages at all the nodes, but rather we'd like to concern about the input-output parameters (such as S-parameter) of the network. Arranging the sequence of unknowns, we can always write the nodal equations in a matrix form

$$\underbrace{\begin{bmatrix} Y_{11} & Y_{12} \\ Y_{21} & Y_{22} \end{bmatrix}}_Y \underbrace{\begin{bmatrix} V_{in} \\ V_{ports} \end{bmatrix}}_V = \underbrace{\begin{bmatrix} 0 \\ I_{ports} \end{bmatrix}}_I, \quad (3.1)$$

where  $V_{in}$  represents internal nodes' voltages, which is a  $n-1-m \times 1$  vector;  $V_{ports}$  represents external nodes' voltages, which is a  $m \times 1$  vector;  $Y_{11}$ ,  $Y_{12}$ ,  $Y_{21}$ ,  $Y_{22}$  are the admittance matrices linking every pair of nodes. After some simple manipulation, the input-output Y-parameter matrix is given by

$$Y\text{-para} = \frac{I_{ports}}{V_{ports}} = Y_{22} - Y_{21}Y_{11}^{-1}Y_{12}. \quad (3.2)$$

Since the matrices in equation (3.2) are filled with frequency-dependent elements, thus Y-parameter is obtained only by sweeping the whole frequency range of interest. However, it is difficult to treat matrix with different function of frequency (such as  $j\omega$  and  $1/j\omega$ ) in a computer-aided circuit solver as well as in mathematical MOR applications. Therefore, SNA method needs slightly modified.

### 3.2.2 General Theory of Modified Nodal Analysis

MNA method is first introduced in [9], which is widely adopted in programmed circuit solvers. In MNA, inductance branches' currents are added into the unknown vectors, which can avoid mixing  $j\omega$  terms with  $1/j\omega$  terms as appeared in SNA. Another advantage of MNA is that nearly all common components can be easily **stamped** into the system matrices, which are convenient to deal with by a computer algorithm. The definition and use of components **stamps** are available in [10].

A basic procedure for MNA is:

- (1). Choosing a node as the datum node (ground node), and numbering the rest of the nodes;

- (2). Numbering all the inductors, and registering the currents that go through voltage sources;
- (3). Applying Kirchhoff current law to each of the nodes;
- (4). Applying the basic Ohm's law to each inductor in terms of its current and nodal voltages applied to both ends; and
- (5). Solving all unknowns: the node voltages and the inductor currents.

Similar to that in SNA, we may concern more about input-output parameters (such as S-parameter) instead of the voltages at all the nodes. An example can easily illustrate how the MNA works.

In Figure 3.1 a two-port network is given: nodes and different type components with their numbers are marked on it. Reference current directions for all inductances are predefined too. Besides, all initial energy stored is assumed to be zero.

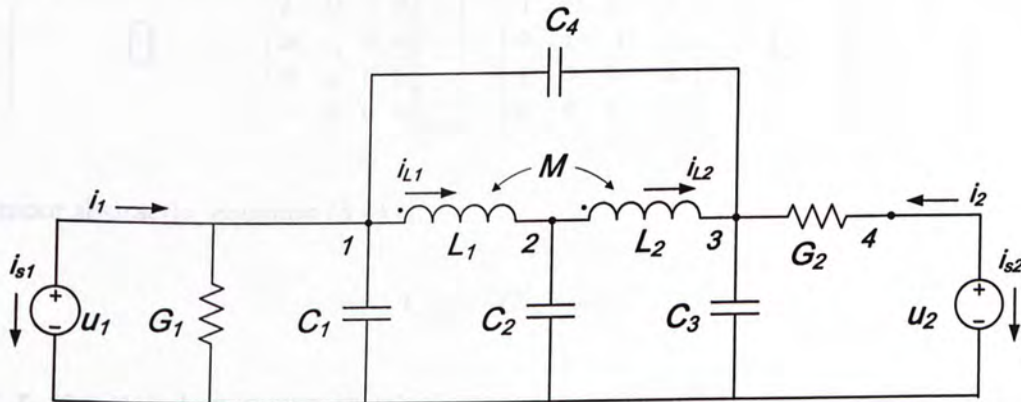


Figure 3.1 Example two-port network.

The unknowns chosen are four node voltages, two inductor currents and two currents from the sources, thus in Laplacian domain, MNA matrix is formed below:

$$\left[ \begin{array}{cccc|cccc}
 G_1 + s(C_1 + C_4) & 0 & -sC_4 & 0 & 1 & 0 & 1 & 0 \\
 0 & sC_2 & 0 & 0 & -1 & 1 & 0 & 0 \\
 -sC_4 & 0 & G_2 + s(C_3 + C_4) & -G_2 & 0 & -1 & 0 & 0 \\
 0 & 0 & -G_2 & G_2 & 0 & 0 & 0 & 1 \\
 \hline
 1 & -1 & 0 & 0 & sL_1 & sM & 0 & 0 \\
 0 & 1 & -1 & 0 & sM & sL_2 & 0 & 0 \\
 1 & 0 & 0 & 0 & 0 & 0 & 0 & 0 \\
 0 & 0 & 0 & 1 & 0 & 0 & 0 & 0
 \end{array} \right] \begin{bmatrix} v_1 \\ v_2 \\ v_3 \\ v_4 \\ i_{L1} \\ i_{L2} \\ i_{s1} \\ i_{s2} \end{bmatrix} = \begin{bmatrix} 0 \\ 0 \\ 0 \\ 0 \\ 0 \\ 0 \\ u_1 \\ u_2 \end{bmatrix}, \quad (3.3)$$

where above the horizontal partition line are nodal equations, and below it are equations for Ohm's law being applied to each inductance branches and equations for ports current/voltage relations. Obviously, the dimension of MNA matrix in equation (3.3) is twice of the matrix formed by SNA method, but the reward is profound: we can separate the frequency variable from the matrix. Now equation (3.3) can be rewritten as

$$\left[ \begin{array}{cccc|cccc}
 C_1 + C_4 & 0 & -C_4 & 0 & & & & \\
 0 & C_2 & 0 & 0 & & & & \\
 -C_4 & 0 & C_3 + C_4 & 0 & & & & \\
 0 & 0 & 0 & 0 & & & & \\
 \hline
 & & & & L_1 & M & 0 & 0 \\
 & & & & M & L_2 & 0 & 0 \\
 & & & & 0 & 0 & 0 & 0 \\
 & & & & 0 & 0 & 0 & 0
 \end{array} \right] \begin{bmatrix} \dot{v}_1 \\ \dot{v}_2 \\ \dot{v}_3 \\ \dot{v}_4 \\ i_{L1} \\ i_{L2} \\ i_{s1} \\ i_{s2} \end{bmatrix} = - \left[ \begin{array}{cccc|cccc}
 G_1 & 0 & 1 & 0 & 1 & 0 & 1 & 0 \\
 0 & 0 & 0 & 0 & -1 & 1 & 0 & 0 \\
 0 & 0 & G_2 & -G_2 & 0 & -1 & 0 & 0 \\
 0 & 0 & -G_2 & G_2 & 0 & 0 & 0 & 1 \\
 \hline
 1 & -1 & 0 & 0 & & & & \\
 0 & 1 & -1 & 0 & & & & \\
 1 & 0 & 0 & 0 & & & & \\
 0 & 0 & 0 & 1 & & & & 
 \end{array} \right] \begin{bmatrix} v_1 \\ v_2 \\ v_3 \\ v_4 \\ i_{L1} \\ i_{L2} \\ i_{s1} \\ i_{s2} \end{bmatrix} + \begin{bmatrix} 0 \\ 0 \\ 0 \\ 0 \\ 0 \\ 0 \\ u_1 \\ u_2 \end{bmatrix}. \quad (3.4)$$

Or more abstractly, equation (3.4) is

$$C\dot{x}_n = -Gx_n + Bu_N, \quad (3.5)$$

where  $x_n$  is a  $n \times 1$  unknown variable-composed vector,  $\dot{x}_n$  is its derivative and  $u_N$  is the source voltages,  $C$  and  $G$  are all  $n \times n$  matrices, and  $B$ 's dimension is  $n \times N$ , where  $N$  is the ports number, and here  $N$  is equal to 2 for a two-port network. Clearly, matrix  $C$  is filled with energy storage elements, such as capacitances and inductances, while matrix  $G$  stores lossy



elements and all inductances' current-voltage relation information elements. Matrix  $B$  indicates the ports voltages' information.

Besides, the relation between the port voltages and their currents is

$$\underbrace{\begin{bmatrix} i_1 \\ i_2 \end{bmatrix}}_{i_N} = \underbrace{\begin{bmatrix} 0 & 0 & 0 & 0 & 0 & 0 & -1 & 0 \\ 0 & 0 & 0 & 0 & 0 & 0 & 0 & -1 \end{bmatrix}}_{B^T} x_n, \quad (3.6)$$

where  $i_1$  and  $i_2$  are shown in Figure 3.1, which are opposite to  $i_{s1}$  and  $i_{s2}$  respectively. They are introduced deliberately for computing output responses.

Solving for the unknowns  $x_n$  from equation (3.5) in Laplacian domain, and substituting them into equation (3.6), one can easily find Y-parameter as:

$$Y(s) = \frac{i_N}{u_N} = B^T (G + sC)^{-1} B. \quad (3.7)$$

After Y-parameter is acquired, without any difficulty, it can be converted into S-parameter by: [11]

$$\begin{aligned} S_{11} &= \frac{(Y_0 - Y_{11})(Y_0 + Y_{22}) + Y_{12}Y_{21}}{(Y_{11} + Y_0)(Y_{22} + Y_0) - Y_{12}Y_{21}}; \\ S_{12} &= \frac{-2Y_{12}Y_0}{(Y_{11} + Y_0)(Y_{22} + Y_0) - Y_{12}Y_{21}}; \\ S_{21} &= \frac{-2Y_{21}Y_0}{(Y_{11} + Y_0)(Y_{22} + Y_0) - Y_{12}Y_{21}}; \\ S_{22} &= \frac{(Y_0 + Y_{11})(Y_0 - Y_{22}) + Y_{12}Y_{21}}{(Y_{11} + Y_0)(Y_{22} + Y_0) - Y_{12}Y_{21}}, \end{aligned} \quad (3.8)$$

where  $Y_0 = 1/Z_0$  is the reciprocal of the characteristic impedance.

### 3.2.3 Calculate the System Poles Using MNA

In addition to find frequency domain responses, we can also use MNA matrices to find out the system poles.

Having had system poles will greatly help to understand a system. In the next chapter of this thesis we will compare system poles before and after physics-based MOR, since this can show the coherence in reduction cycles.

The definition of system poles can be found in [13], and the procedure is as follows.

First, set  $s = s_0 + \sigma$ , where  $s_0$  is a fixed complex frequency point. Then build two new matrices  $A$  and  $R$  from the obtained MNA matrices [3]:

$$\begin{aligned} A &= -(G + s_0 C)^{-1} C, \\ R &= (G + s_0 C)^{-1} B. \end{aligned} \quad (3.9)$$

Substitute  $A$  and  $R$  into equation (3.7). After some simple manipulation, the Y-parameter is obtained:

$$Y(s_0 + \sigma) = B^T (I - \sigma A)^{-1} R, \quad (3.10)$$

where  $I$  is an  $n \times n$  identity matrix.

Diagonalizing matrix  $A$ , we have

$$A = S \Lambda S^{-1}, \quad (3.11)$$

where  $\Lambda = \text{diag}(\lambda_1, \lambda_2, \dots, \lambda_n)$  is a diagonal matrix, whose diagonals are the eigenvalues of  $A$ ;  $S$  is the eigen space of  $A$ . Then equation (3.10) has changed to

$$Y(s_0 + \sigma) = B^T (I - \sigma S \Lambda S^{-1})^{-1} R. \quad (3.12)$$

Be reminded that  $I = S^{-1}S$ , equation (3.12) becomes

$$\begin{aligned} Y(s_0 + \sigma) &= B^T S (I - \sigma \Lambda)^{-1} S^{-1} R \\ &= f^H (I - \sigma \Lambda)^{-1} g, \end{aligned} \quad (3.13)$$

where  $f = B^T S$ ,  $g = S^{-1} R$ . Since complex entities may be encountered, conjugate transpose is performed in equation (3.13), which is indicated by superscript  $H$ .

In [6], they didn't use the same form of  $A$  and  $R$  as defined here in equation (3.9). Thus at the lossless or low loss situations,  $A$  might be extremely ill conditioned, therefore, it cannot be guaranteed diagonalizable. Further, the choice of  $s_0$  is critical to MOR scheme which will be introduced later, for matrix  $A$  also relates to the creation of Krylov subspace. In the implementation,  $s_0$  is chosen to be within  $2\pi f_{\min} \sim 2\pi f_{\max}$ , where  $f_{\min}$  is the lowest frequency of interest and  $f_{\max}$  is the highest. Detail theory on  $s_0$  selection is available in [3].

With quadratic form knowledge, a more practical form is written from equation (3.13):

$$Y(s_0 + \sigma) = \sum_{j=1}^n \frac{f_j g_j}{1 - \sigma \lambda_j}. \quad (3.14)$$

Clearly,  $1 / \lambda_j + s_0$  is the expression for system pole, where  $j = 1, 2, \dots, n$ . For a passive circuit, the entire poles should be located within the left half of the complex plane.

### 3.2.4 Examples and Comparisons

A simple square spiral inductor design is shown in Figure 3.2.

## 3.3 Krylov Subspace MOR Method

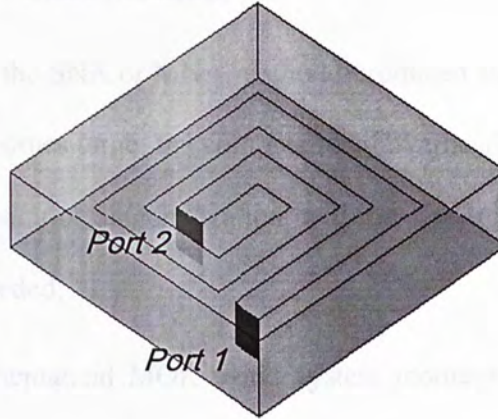


Figure 3.2 Planar spiral inductor.

After MNA analysis, system poles are obtained, which are all pure imaginary numbers, showing in the table below.

Table 3.1 System poles.

No.	Im (Sys. Poles)
1	9.19
2	14.63
3	21.72
4	26.54
5	29.31
6	39.35
7	43.34
8	48.29
9	52.26
10	59.29
11	62.89
12	83.51
13	97.57
14	124.88
15	115.95

The system poles shown are normalized to  $10^{-9}$  and their conjugates are not shown in Table 3.1 for the sake of clarity. More examples will be shown in chapter 4.

### 3.3 Krylov Subspace MOR Method

For a small scale system, the SNA or MNA method introduced above is quite fast. However, when the circuit scale becomes large, the computational overhead for the matrices manipulation, such as matrix inversion or diagonalization, will increase tremendously. Thus, an effective MOR technique is needed.

In early stages of mathematical MOR work, system moments matching and Padé's approximation method [2] are utilized, from which a smaller state-space preserving a certain number of original poles can be achieved. But due to its explicit moment calculation scheme, the accuracy of [2] cannot be guaranteed [3]. Thus, researchers are turning to Krylov subspace MOR techniques.

There are many different MOR schemes based on Krylov subspace. However, the core idea is more or less the same: A large system is reasonably projected onto a small system.

The original state-space of a circuit is described in equation (3.5) and (3.6), and we repeat them here for convenience:

$$\begin{aligned} C\dot{x}_n &= -Gx_n + Bu_N \\ i_N &= B^T x_n, \end{aligned} \quad (3.15)$$

where  $n$  is the original vector  $x_n$ 's dimension. Assume another much smaller state-space only have  $q$  unknowns. If an  $n \times q$  sized transfer-space  $X$  could be found out, then all the MNA matrices in equation (3.15) can be transformed into a new state-space by pre/post multiplication of  $X$ :

$$\begin{aligned} \tilde{C}\dot{x}_q &= -\tilde{G}x_q + \tilde{B}u_N \\ i_N &= \tilde{B}^H x_q, \end{aligned} \quad (3.16)$$

where  $x_q$  is the new unknowns vector, and

$$\tilde{C}_{q \times q} = X_{n \times q}^H C_{n \times n} X_{n \times q}; \quad \tilde{G}_{q \times q} = X_{n \times q}^H G_{n \times n} X_{n \times q}; \quad \tilde{B}_{q \times 2} = X_{n \times q}^H B_{n \times 2}. \quad (3.17)$$

The subscripts in (3.17) denote the dimension information of the matrices. Obviously, the dimension of the new state-space is greatly reduced by nearly  $n / q$  times. From this new state-space, the frequency domain output responses can be calculated out very quickly. Further, if stamping those matrices shown in (3.17) directly to some capable MNA solver, time-domain responses can also be found out.

For different schemes, there are different ways to calculate the transfer-space  $X$ , however they all exploit Krylov subspace method. In this work, we only use one of the most efficient algorithms to build the Krylov subspace, upon which matrix  $X$  is found.

If the desired dimension for the reduced model is  $q$ , which is commonly several orders smaller than the original dimension  $n$ . Then for  $A$  and  $R$  defined in (3.9), where  $A \in \mathbb{C}^{n \times n}$  and  $R = [r_0, r_1] \in \mathbb{C}^{n \times 2}$ , the generated Krylov subspace is: [5][6]

$$\begin{aligned} Kr(A, R, q) &\equiv \text{colsp} [R, AR, A^2R, \dots, A^k R] && \text{if } k \text{ is even;} \\ Kr(A, R, q) &\equiv \text{colsp} [R, AR, A^2R, \dots, A^k R, A^k r_0] && \text{if } k \text{ is odd,} \end{aligned} \quad (3.18)$$

where  $k = \lfloor q / 2 \rfloor$ , and  $\text{colsp}$  stands for column space.

Transfer-matrix  $X$  is a unitary matrix that spans  $Kr(A, R, q)$ :

$$\begin{aligned} \text{colsp}(X) &= Kr(A, R, q) \\ X_{n \times q}^H X_{n \times q} &= I_{q \times q}. \end{aligned} \quad (3.19)$$

In practical programming, we have utilized QR factorization codes. Detailed procedure and pseudo-code for finding  $X$  are available in [5][12].

Another important issue of this MOR technique is its passivity preservation. Since the target circuit model is commonly passive and consequently a passive reduced model is also expected. Fortunately, the above MOR process has been proved to be stable and passive [6], thus it is not a concern here.

### 3.4 Examples of Krylov Subspace MOR

First, the example used in chapter 2 PEEC modeling is repeated here for showing the effect of mathematical MOR. The circuit layout of the design is originally shown in Figure 2.6, and the geometry parameters can be found in section 2.5. The calculated S-parameter from the reduced model and the original model are compared below:

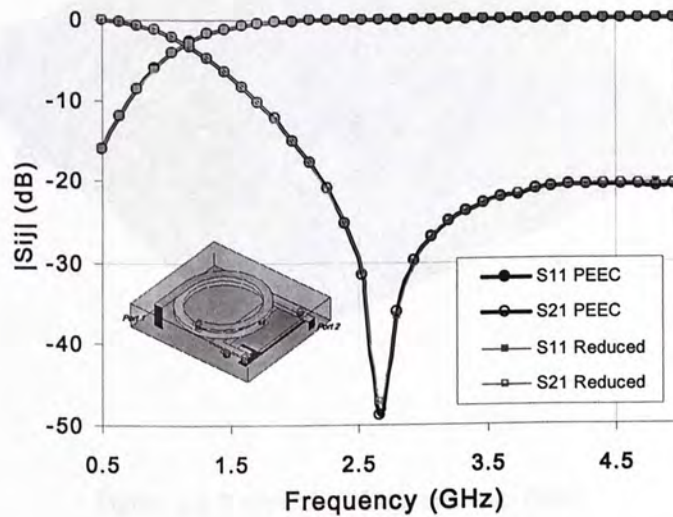


Figure 3.3 S-parameters comparison between the original model and the mathematical MOR model of a LTCC low-pass filter.

The original dimension of system matrix built from PEEC modeling is  $131 \times 131$ . However, the reduced macromodel can have a dimension of only  $12 \times 12$ . The expansion point  $s_0$

is chosen to be  $2\pi \times 10^9$ . Clearly in Figure 3.3, two pairs of curves from two models match well in the frequency range up to 5GHz.

The second example given is a typical microstrip filter. Though the layout looks simple, it works up to 12GHz.

The dielectric box enclosing the design is  $30\text{mm} \times 30\text{mm} \times 0.79\text{mm}$ , and the strip has a width of 2.54mm. A network composed by 946 capacitors, 390 inductors with 5005 mutual couplings is extracted. Correspondingly,  $618 \times 618$  MNA matrices have been formed.

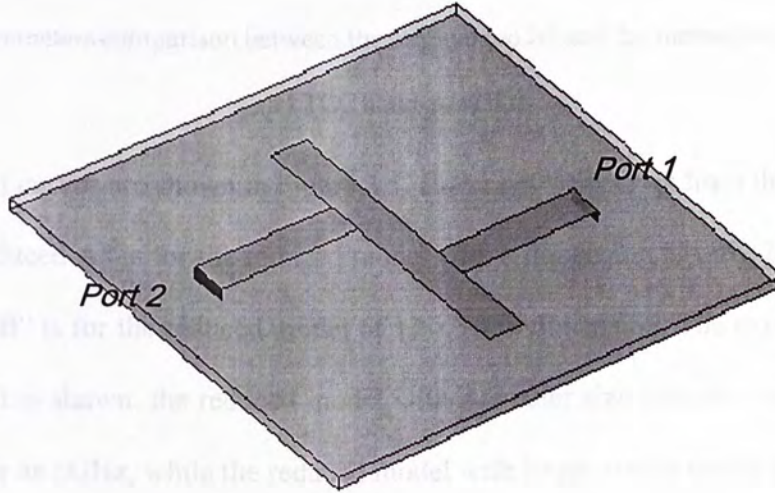


Figure 3.4 A typical LTCC band-stop filter.

The effect of different size of reduced models can be seen in Figure 3.5.



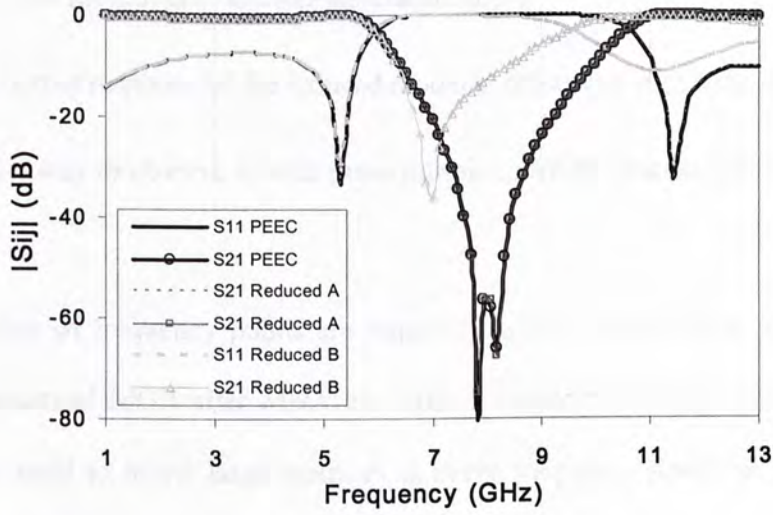


Figure 3.5 S-parameters comparison between the original model and the mathematical MOR model of a LTCC band-pass filter.

Three sets of curves are shown in Figure 3.5. Curve set “PEEC” is from the original model; curve set “Reduced A” is for the reduced model with a dimension of only  $24 \times 24$ , and curve set “Reduced B” is for the reduced model of  $12 \times 12$  in dimension. The expansion point  $s_0$  is  $2\pi \times 10^9$ . As it is shown, the reduced model with a smaller size can only match the original model to as far as 6GHz, while the reduced model with larger size is nearly identical with the original model over the entire frequency range.

### 3.5 Summary

In this chapter, the basic concept of a mathematics-based MOR scheme and its application to simplify a PEEC circuit model is given.

The reason we incorporate this Krylov subspace MOR method with our PEEC modeling technique is

- (1). This MOR scheme can give a faster simulation speed.
- (2). The input-output response of the reduced model is preserved with little distortion.
- (3). It provides a way to observe system poles during an MOR process (illustrated in chapter 4).

If a large number of frequency points are required, usually over a fairly wide frequency range, the mathematical MOR after MNA can offer a considerably high simulation speed, since it does not need to invert large matrices at every frequency points as other methods based on equation (3.2).

The shortcoming of the mathematical MOR scheme is also apparent. We are unable to restore a circuit from equation (3.16) that describes a reduced state-space. Unlike the matrices in equation (3.4), equation (3.16) are composed of dense matrices with complex-valued entries. Therefore the reduced model has lost all its physical meaning which used to be included in the original model.

In order to overcome the shortcomings above, we are going to investigate physics-based MOR schemes in the next chapter, from which a realizable reduced model can be generated.

## References

- [1] B. C. Moore, "Principal component analysis in linear systems: controllability, observability, and model reduction," *IEEE Trans. Automat. Contr.*, vol. AC-26, pp.17-23, Feb. 1981.
- [2] L. T. Pillage and R. A. Rohrer, "Asymptotic waveform evaluation for timing analysis," *IEEE Trans. Computer-Aided Design*, vol. 9, pp. 352-366, April 1990.

- [3] P. Feldmann and R. W. Freund, "Efficient linear circuit analysis by Padé approximation via the Lanczos process," *IEEE Trans. Computer-Aided Design*, vol. 14, pp. 639-649, May 1995.
- [4] P. Feldmann and R. W. Freund, "Reduced-order modeling of large linear subcircuits via a block Lanczos algorithm," in *IEEE/ACM Proc. DAC*, June 1995, pp. 474-479.
- [5] D. L. Boley, "Krylov space methods on state-space control models," *Circuits Syst. Signal Processing*, vol. 13, no. 6, pp. 733-758, 1994.
- [6] A. Odabasioglu, M. Celik, and L. T. Pillage, "PRIMA: Passive reduced-order interconnect macromodeling algorithm," *IEEE Trans. Computer-Aided Design*, vol. 17, pp. 645-654, Aug. 1998.
- [7] K. J. Kerns and A. T. Yang, "Stable and efficient reduction of large, multiport RC networks by pole analysis via congruence transformation," *IEEE Trans. Computer-Aided Design*, vol. 16, pp. 734-744, July 1997.
- [8] G. Rizzoni, "*Principles and Applications of Electrical Engineering*," Boston: McGraw-Hill, 2003.
- [9] C. W. Ho, A. E. Ruehli, and P. A. Brennan, "The modified nodal approach to network analysis," *IEEE Trans. Circuits Syst.*, vol. CAS-22, pp. 504-509, June 1975.
- [10] J. Vlach, "*Basic Network Theory with Computer Applications*," New York: Van Nostrand Reinhold, 1992, ch.17.
- [11] D. M. Pozar, "*Microwave engineering*," Hoboken, NJ: John Wiley, 2005, ch. 4.
- [12] D. L. Boley and G. H. Golub, "The nonsymmetric Lanczos algorithm and controllability," *Systems Control Lett.* vol. 4, pp. 317-324, 1984.

- [13] D. F. Tuttle, Jr., “*Electric Networks; Analysis and Synthesis*,” New York : McGraw-Hill, 1965.

## Chapter 4

## PHYSICAL MODEL ORDER REDUCTION

## 4.1 Introduction

In last chapter, the principle of mathematical-based MOR is presented, and the disadvantages of it is also discussed. Undoubtedly, mathematical MOR has greatly decreased the simulation time. Nevertheless, the mathematical MOR techniques do not meet many practical requirements for the following reasons: (1) the excessive nodes and components in the original circuit significantly reduces the efficiency of the circuit solver, even if mathematical MOR is applied. (2) Not all of the circuit solvers are capable of recognizing the macromodels generated by the mathematical MOR [1]. As shown in last chapter, a system matrix after mathematical MOR becomes dense and lacks of physical meanings. There are few circuit solvers that can read and solve a mathematical MOR resultant matrix. (3) A succinct, physically meaningful and accurate circuit representation would provide physical insight of a circuit, and it is the ultimate goal of many RF layout designers. S-parameters may provide some functionalities of a circuit, but lack of valuable physical understanding that only a circuit model can provide. Such physical information is indispensable during the essential design period.

Some researchers have tried to use a simple pre-defined circuit model to fit the original circuit [13-15]. Such “fitting” requires a priori knowledge on the parameters of both the circuit to be fitted and the circuit model. To develop a systematic method that can generate a physically expressive circuit model, as introduced in chapter 2, the POC algorithm, which can be regarded as a generic mesh-dependant original circuit model, is adopted as the surrogate

## Chapter 4

# PHYSICAL MODEL ORDER REDUCTION

### 4.1 Introduction

In last chapter, the principle of mathematics-based MOR is presented, and the disadvantage of it is also discussed. Undoubtedly, mathematical MOR has greatly decreased the simulation time. Nevertheless, the mathematical MOR techniques do not meet many practical requirements for the following reasons: (1) the excessive nodes and components in the original netlist significantly reduces the efficiency of the circuit solver, even if mathematical MOR is applied. (2) Not all of the circuit solvers are capable of recognizing the macromodels generated by the mathematical MOR [1]. As shown in last chapter, a system matrix after mathematical MOR becomes dense and lacks of physical meanings. There are few circuit solvers that can read and solve a mathematical MOR resultant matrix. (3) A succinct, physically meaningful and accurate circuit representation would provide physical insight of a circuitry and is the ultimate goal of many RF layout designers. S-parameters may provide some features of a circuit, but lack of valuable physical understanding that only a circuit model contains. Such physical information is indispensable during the conceptual design period.

Some researchers have tried to use a simple pre-defined circuit model to fit their layout design [2]-[4]. Such ‘fitting’ requires a priori knowledge on the performance of both the circuit layout to be fitted and the circuit model. To develop a systematic method that can derive a physically expressive circuit model, as introduced in chapter 2, the PEEC algorithm, which is able to generate a generic mesh-dependant original circuit model, is adopted as the starting

point. Since the original circuit model generated is always excessively complicated for any practical use, we will focus on simplifying the original circuit model, i.e. using a physics-based MOR scheme to get a concise and physically meaningful circuit model with pivotal attributes inherited from its earliest original circuit layout. Recently, the basic concept of the physical MOR for lossless circuits has been proposed in [5]. When dealing with the circuits with practical losses, although some research was done [6], a more general and simple methodology for complex circuit elements needs to be developed.

This chapter starts from the discussion of Gaussian elimination to the SNA equations (introduced in chapter 3). The lossy models for the capacitive and inductive cells are then proposed. With the lossy models, two different processes for the MOR are presented. Finally examples demonstrating the effectiveness of the physically expressive MOR methods are given.

## 4.2 Gaussian Elimination Method

Traditional Gaussian elimination method is an algorithm in linear algebra for determining the solutions to a large number of linear equations. The algorithm works by first rearranging the augmented rectangular matrix that describes the linear equations into reduced row echelon forms, and then solving for the unknown from the bottom row with the right-most pivot to the top most rows. The obtained solution is back-substituted to the rest of the equations for solving the following unknown [7], and finally all the unknowns are found out.

This linear algebra algorithm can be performed to simplify a circuit due to the fact that a lumped circuit can always be written in linear nodal equation forms, i.e. the SNA equation

form shown in chapter 3. The rationale behind the Gaussian elimination in nodal analysis is introduced in details below.

As shown in Figure 4.1, a typical four-node lumped network is composed by *RLC* elements. Node 1 and node 2 are internal nodes, while node 3 and node 4 are port nodes.

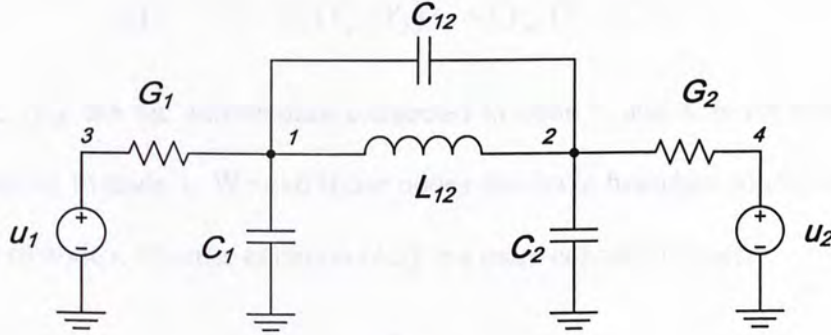


Figure 4.1 A simple four-node circuit network.

The node equation in Laplacian domain for node 1 can be expressed as

$$sC_1V_1 + (sC_{12} + L_{12}/s)(V_1 - V_2) + G_1(V_1 - V_3) = 0. \quad (4.1)$$

Equation (4.1) is based on Kirchhoff Current Law, where  $V_1-V_3$  are node voltages,  $s$  is the complex frequency variable which equals to  $j\omega$ .

Therefore, a set of four SNA equations describing the whole circuit can be written in matrix format as below:

$$\begin{bmatrix} G_1 + s(C_{12} + C_1) + L_{12}/s & -sC_{12} - L_{12}/s & -G_1 & 0 \\ -sC_{12} - L_{12}/s & G_2 + s(C_{12} + C_2) + L_{12}/s & 0 & -G_2 \\ -G_1 & 0 & G_1 & 0 \\ 0 & -G_2 & 0 & G_2 \end{bmatrix} \begin{bmatrix} V_1 \\ V_2 \\ V_3 \\ V_4 \end{bmatrix} = 0. \quad (4.2)$$

On a given frequency point, (4.2) are just the linear equations one can apply the Gaussian elimination for solving the unknown node voltages. However, we do not need to solve for all

the unknowns, but preferably, we substitute one solved node voltage into all the other equations and establish a new circuit model.

More generically, if a network consisting of  $N$  nodes, a total of  $N$  nodal equations similar to equation (4.2) can be formulated. The equation for node  $x$  in those  $N$  equations is

$$y_{x1}(V_x - V_1) + y_{x2}(V_x - V_2) + \dots + y_{xK}(V_x - V_K) = 0, \quad (4.3)$$

where  $y_{x1}, y_{x2}, \dots, y_{xK}$  are the admittances connected to node  $x$ , and  $K$  is the total number of nodes that connect to node  $x$ . We call those nodes that have branches connecting to node  $x$  the **neighbors** of node  $x$ . Rewrite equation (4.3) in a more concise manner:

$$Y_{tx}V_x - \sum_{i=1}^K y_{xi}V_i = 0, \quad (4.4)$$

where  $Y_{tx} = \sum_{i=1}^K y_{xi}$ , is the summation of all the admittances connecting to node  $x$ .

In order to eliminate node  $x$  from the circuit, or in other words, to eliminate  $V_x$  from the nodal equations, Gaussian elimination is adopted here. Solving for  $V_x$ , we have:

$$V_x = -\frac{\sum_{i=1}^K y_{xi}V_i}{Y_{tx}}. \quad (4.5)$$

Substitute (4.5) into all the other equations where  $V_x$  appears, for example, the  $m^{\text{th}}$  equation:

$$y_{mx}(V_m - V_x) + y_{m1}(V_m - V_1) + y_{m2}(V_m - V_2) + \dots + y_{mK}(V_m - V_K) = 0, \quad (4.6)$$

where  $M$  other nodes besides node  $x$  have connected to node  $m$ , then it becomes:



$$y_{mx} \left( V_m - \frac{\sum_{i=1}^K y_{xi} V_i}{Y_{tx}} \right) + \left( Y_{tm} V_m - \sum_{j=1}^M y_j V_j \right) = 0. \quad (4.7)$$

In equation (4.7),  $Y_{tm}$  is the summation of admittances connecting from the other  $M$  nodes to node  $m$ . Separating  $V_m$  term from  $V_x$ 's expression in (4.5) and rearranging (4.7), we have

$$y_{mx} \left( V_m - \frac{y_{xm} V_m + \sum_{i=1, i \neq m}^K y_{xi} V_i}{Y_{tx}} \right) + \left( Y_{tm} V_m - \sum_{j=1}^M y_j V_j \right) = 0. \quad (4.8)$$

Be reminded that  $Y_{tx} = \sum_{i=1}^K y_{xi}$ , then equation (4.8) finally becomes

$$\left( \frac{\sum_{i=1, i \neq m}^K y_{mx} y_{xi} V_m}{Y_{tx}} - \frac{\sum_{i=1, i \neq m}^K y_{mx} y_{xi} V_i}{Y_{tx}} \right) + \left( Y_{tm} V_m - \sum_{j=1}^M y_j V_j \right) = 0. \quad (4.9)$$

The new nodal equation for node  $m$  now has two parts: the first part (terms in the first pair of parentheses in equation (4.9)) indicates that there are new components added in between node  $m$  and nodes which used to be node  $i$ 's neighbors, i.e. node 1, node 2, ..., node  $K$ . The value for the newly added component, is

$$y_{mi} = \frac{y_{mx} y_{xi}}{Y_{tx}}, \quad i = 1, 2, \dots, K; \quad (4.10)$$

the second part (terms in the second pair of parentheses in equation (4.9)) indicates all the other branches that link node  $m$  up with its former neighbor nodes (in addition to node  $x$ ) stay the same as before.

Similar results can be obtained when substituting  $V_x$  into all the other equations, which indicates new components are added between every pair of nodes that used to be node  $x$ 's neighbors. A generic expression for this new component  $y_{mn}$ , which we call **adjoining admittance**, is

$$y_{mn} = \frac{y_m y_n}{Y_{tx}}, \tag{4.11}$$

where  $y_m$  and  $y_n$  are both admittances used to be in between the node  $x$  and its neighbors;  $Y_{tx}$  is the summation of all the admittances connecting to node  $x$ . Consequently, not only variable  $V_x$  is eliminated from the nodal equations, but a new circuit topology with adjoining admittances shown in (4.11) is also recovered.

If the total nodes number of the original circuit is four, this Gaussian elimination process turns out to be the famous  $Y$ - $\Delta$  transformation as shown in Figure 4.2.

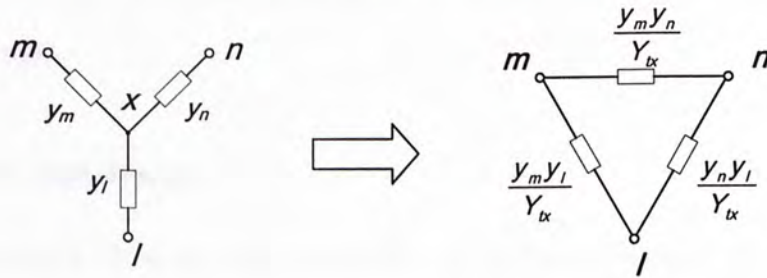


Figure 4.2  $Y$ - $\Delta$  transformation.

In Figure 4.2,  $x$  is the node to be eliminated;  $m$ ,  $n$ , and  $l$  are the neighbors of node  $x$ . After elimination, adjoining admittances are added in between every pair of three former neighbors of node  $x$ .

Once the equivalent circuit topology is obtained after a node being removed, one needs to simplify the resultant circuit such that the other insignificant nodes can be ‘absorbed’ by a recursive process.

In order to extend the developed physically expressive MOR method from lossless application to lossy cases, we first need to prepare a PEEC circuit model that can involve all the apparent losses under the quasi-static approximation before investigating systematic MOR methodologies for lossy circuit layouts.

### 4.3 A Lossy PEEC Circuit Model

The existing quasi-static PEEC model only extracts two types of components: inductance  $L$  and capacitance  $C$  for a lumped circuit network. When analyzing a lossy multilayered circuit, one needs to consider two types of lossy elements: conductor loss associated to an inductance and substrate loss that can be represented by a conductance in shunt with a capacitance with respect to the ground.

#### 4.3.1 Loss with Capacitance

To accurately calculate the conductance associated to the substrate loss is not easy. Since the cases considered are quasi-static layered structures surrounded by homogeneous dielectric media, one can adopt a simple way in classic electromagnetic text book [8] to approximately calculate the conductance.

$$G_c = \frac{\sigma C}{\varepsilon}. \quad (4.12)$$

Where  $\sigma$  is the conductivity of the lossy dielectric,  $C$  is the capacitance and  $\epsilon$  is the dielectric constant.

Equation (4.12) implies that once we know the capacitance with respect to the ground, the conductance  $G_C$  associated to substrate loss can be determined immediately. It should be noted that the  $C$  is in shunt with the  $G_C$  as shown in Figure 4.3.

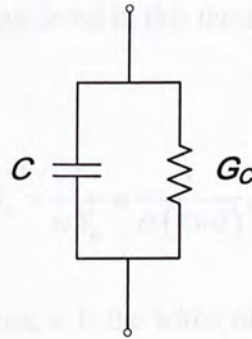


Figure 4.3 Capacitance and its loss.

This simple way for incorporating the substrate loss is easy to implement in a PEEC model since the capacitance of a capacitor cell with respect to the ground can be easily obtained in a PEEC model.

It is noted that the  $\epsilon/\sigma$  ratio for a given substrate can be obtained from the expression of the material's loss tangent:

$$\tan \delta_c \cong \frac{\sigma}{\omega \epsilon}, \quad (4.13)$$

where  $\omega$  is the angular frequency. Therefore, the capacitance's loss is now available.

### 4.3.2 Loss with Inductance

The conductor loss is significant for the circuits in which the current distribution dominantly determines the circuit performance. For example, in a planar spiral inductance layout, the metal loss is especially important [9]-[11] and needs to be correctly reflected in the circuit model derivation. Other studies on conductor loss can be found in [14]-[21].

Assuming the inductive meshes considered in this thesis are all in regular shapes, the resistance can be approximated by:

$$R_L = \frac{l}{\sigma S_e} = \frac{l}{\sigma(2w\delta)}, \quad (4.14)$$

where  $S_e$  is the equivalent crossing area,  $w$  is the width of the strip,  $l$  is the length of the strip and  $\delta$  is the skin depth.

If a typical thickness of copper layer is about  $12 \mu\text{m}$  (0.5 mil), when the circuit operates at 2 GHz the skin depth  $\delta$  is equal to  $1.48 \mu\text{m}$  (0.06 mil).

The circuit model of an inductance with conductor loss is shown in Figure 4.4.



Figure 4.4 Inductance and its loss.

Even though several factors have been omitted in this loss model, such as the proximity effect and eddy current effect [11][12], this inductance loss model has shown to be able to give a satisfactory accuracy.

#### 4.4 Conversion of Mutual Inductive Couplings

Mutual inductances are inevitable among a multilayered circuit and are presented in the PEEC model. There are two different ways to express the mutual couplings in a circuit: (1) **mutual inductance**, illustrated in Figure 4.5, is a measure of the coupling between two inductors. Usually it is indicated as  $M$ ; and (2) **inter-inductance**, indicated as  $L$ , which is no different from other self-inductances, is just a direct inductance whose two terminals are connected to two nodes in the network. The illustration for inter-inductance is Figure 4.6, where  $L'_{13}$ ,  $L'_{24}$ ,  $L'_{14}$  and  $L'_{23}$  are the inter-inductances. Since it is not straightforward to apply the  $Y-\Delta$  transformation to a circuit containing mutual inductances, we need to convert a network that contains mutual inductances to a network that contains only direct self-inductances. The principle of this conversion is based on the equivalence of the Y-matrix of the mutual inductance circuit and that of a self-inductance circuit [13]. A simple example is given below to demonstrate this process.

A simple two-port circuit with a pair of coupled inductances is shown in Figure 4.5.

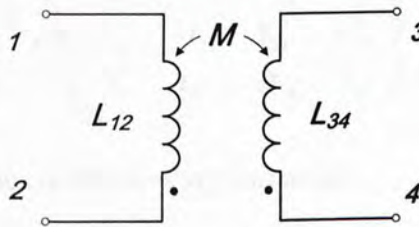


Figure 4.5 A pair of coupled inductances.

The Z-parameter equation of the network is

$$\begin{bmatrix} V_{12} \\ V_{34} \end{bmatrix} = \begin{bmatrix} V_1 - V_2 \\ V_3 - V_4 \end{bmatrix} = j\omega \begin{bmatrix} L_{12} & M \\ M & L_{34} \end{bmatrix} \begin{bmatrix} I_{12} \\ I_{34} \end{bmatrix}, \quad (4.15)$$

where  $M$  is the mutual inductance,  $V_{12}$  and  $V_{34}$  are the voltage drops on the inductances,  $V_1, \dots, V_4$  are the four node voltages,  $I_{12}$  and  $I_{34}$  are currents going through  $L_{12}$  and  $L_{34}$  respectively.

Inverting the Z-matrix in equation (4.15), Y-matrix can be obtained:

$$\begin{bmatrix} I_{12} \\ I_{34} \end{bmatrix} = \frac{1}{j\omega} \begin{bmatrix} Y_{11} & Y_{12} \\ Y_{21} & Y_{22} \end{bmatrix} \begin{bmatrix} V_1 - V_2 \\ V_3 - V_4 \end{bmatrix}. \quad (4.16)$$

Obviously,  $Y_{12}$  equals to  $Y_{21}$ .

Equation (4.16) can be rearranged and expressed in another way:

$$\begin{bmatrix} I_{12} \\ -I_{12} \\ I_{34} \\ -I_{34} \end{bmatrix} = \frac{1}{j\omega} \begin{bmatrix} Y_{11} & -Y_{11} & Y_{12} & -Y_{12} \\ -Y_{11} & Y_{11} & -Y_{12} & Y_{12} \\ Y_{21} & -Y_{21} & Y_{22} & -Y_{22} \\ -Y_{21} & Y_{21} & -Y_{22} & Y_{22} \end{bmatrix} \begin{bmatrix} V_1 \\ V_2 \\ V_3 \\ V_4 \end{bmatrix}. \quad (4.17)$$

or

$$\begin{bmatrix} I_1 \\ I_2 \\ I_3 \\ I_4 \end{bmatrix} = \frac{1}{j\omega} \begin{bmatrix} Y_{11} & -Y_{11} & Y_{12} & -Y_{12} \\ -Y_{11} & Y_{11} & -Y_{12} & Y_{12} \\ Y_{21} & -Y_{21} & Y_{22} & -Y_{22} \\ -Y_{21} & Y_{21} & -Y_{22} & Y_{22} \end{bmatrix} \begin{bmatrix} V_1 \\ V_2 \\ V_3 \\ V_4 \end{bmatrix}, \quad (4.18)$$

in which  $I_i$  ( $i=1,2,3$  and  $4$ ) is the current flowing into node  $i$ .

From equation (4.18), the corresponding network containing only self-inductances can be determined:

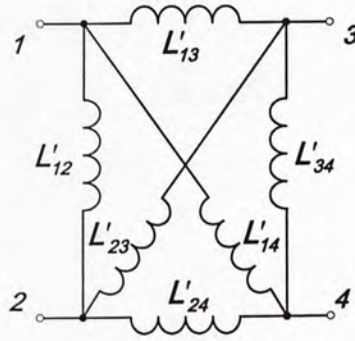


Figure 4.6 The equivalent non-coupled inductance network.

In Figure 4.6,  $L'_{12} = \frac{1}{Y_{11}}$ ,  $L'_{34} = \frac{1}{Y_{22}}$ ,  $L'_{13} = L'_{24} = -\frac{1}{Y_{12}}$  and  $L'_{14} = L'_{23} = \frac{1}{Y_{12}}$ .

As the value of an mutual inductance must be smaller (usually two orders' smaller) than that of the primary pair of self-inductances, the absolute value of  $L'_{13}$ ,  $L'_{24}$ ,  $L'_{14}$  and  $L'_{23}$  must be much greater than  $L'_{12}$  or  $L'_{34}$ , and the obtained  $L'_{12}$  and  $L'_{34}$  may have only slightly variations to  $L_{12}$  and  $L_{34}$  in Figure 4.1, respectively. To distinguish the resultant non-coupled self-inductances, we call  $L'_{12}$  and  $L'_{34}$  **main inductances**, because they are descent from the original self-inductances. We call  $L'_{13}$ ,  $L'_{24}$ ,  $L'_{14}$  and  $L'_{23}$  **inter-inductances**, because they mainly depend on the mutual inductances.

As can be noticed, some of the inter-inductances are negative. These negative inductances will not bring up any instability issues in the circuit solution. This is because there is no approximation made in the conversion process; all the inter-inductances can be converted back to the original indirect mutual inductances.

If the loss factor is considered, the resistances calculated in section 4.3.2 will be superimposed to the main inductances, for they are directly derived from the corresponding inductive



meshes from which the loss originates. Therefore, having added lossy elements to the main inductances, the direct mutual inductance circuit model can be presented by Figure 4.7.

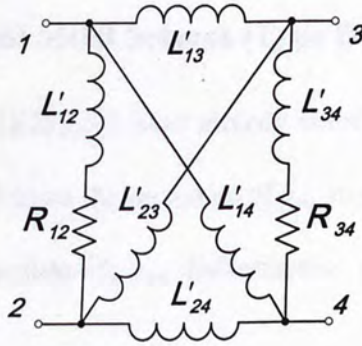


Figure 4.7 Lossy equivalent non-coupled inductances.

The conversion process presented above can be extended to any complicated multi-nodes coupled networks.

#### 4.5 Model Order Reduction Schemes

After lossy PEEC model has been prepared, then we need to recursively reduce and simplify our circuit model. In this section, two simplification schemes for lossy multilayered circuits are proposed. Both of these two schemes are originated from Gaussian elimination method, but they have employed different ways to enable recursive MOR. **Type I MOR** is based on Taylor expansion technique. **Type II MOR** is more ingenious: with the concept of complex-valued inductance and capacitance, the adjoining admittance  $y_{mn}$  is expanded to derive a physically expressive equivalent circuit to facilitate the whole MOR process.

Since the adjoining admittance  $y_{mn}$ , which is introduced in  $Y-A$  transformation, will be the core term in MOR process to be dealt with, thus it is rewritten here for convenience:

$$y_{mn} = \frac{y_m y_n}{Y_{ix}}. \quad (4.19)$$

### 4.5.1 Taylor Expansion Based MOR Scheme (Type I)

A number of previous work [22][23][24] have already considered the use of Taylor expansion (or power expansion) to calculate the moments of  $y_{mn}$  in equation (4.19). By keeping the appropriate moments, people can simplify  $y_{mn}$ . Nevertheless, much improvement needs to be made.

In [23], only limited *RC* cases are considered; whereas [24] only focused on moments' extraction and the examples given are irrelevant to MOR. In [22], though *RLC* circuits are considered, the whole reduction scheme is actually based on study *RL* case and *RC* case separately. Besides, in [22] the approximation rules are given without convincing reasons, especially those cases which involve lossy inductances. Therefore, a more rigorous approximation method to equation (4.19) using Taylor expansion needs to be developed.

However, before coming to the MOR part, we still have deal with some problems.

#### 4.5.1.1 Basic Electrical Components in Type I MOR

For lossless cases, the basic electrical components are the capacitance and inductance, which means if any two nodes in a network to be simplified are connected by a branch, this branch must only contain either a capacitance or an inductance, or a capacitance in shunt with an inductance.

Similarly, for lossy cases, only slight changes need to make. The capacitance is now in shunt with a conductance and the inductance is in series with a resistance, which is shown in Figure 4.8.

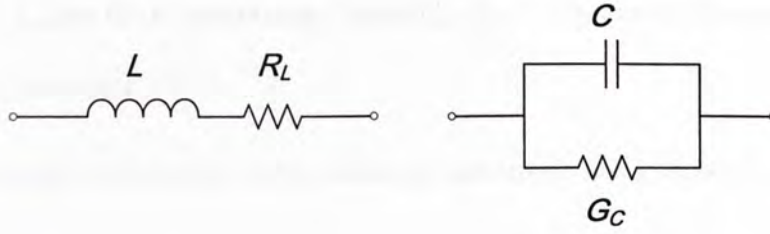


Figure 4.8 Basic electrical components for the lossy circuit.

In order to continuously perform MOR, we need to simplify the adjoining admittance  $y_{mn}$ . Because without any simplification on equation (4.19) in a MOR process, the term  $y_{mn}$  becomes a more and more complicated function of complex frequency and could not be represented by the combination of basic electrical components. Therefore, one needs to find a legitimate approach to simplify the term  $y_{mn}$  so that only basic components need to be dealt with in each step of MOR.

#### 4.5.1.2 Combination of the Lossy Inductances

If no loss appears, such as the circuit extracted from low-loss layout, the approximation rules to  $y_{mn}$  which employed in [5] can be directly applied to Type I MOR. However, if resistance with the inductance must be taken into account, the rules for simplifying  $Y_{ix}$  in (4.19) have to be made first.

As we have noticed in the denominator of (4.19),  $Y_{ix}$  is the summation of the admittances connected to the node to be eliminated, say node  $x$ . For a typical lossless case,  $Y_{ix}$  is:

$$\begin{aligned}
 Y_{ix} &= \frac{1}{j\omega L_1} + \frac{1}{j\omega L_2} + \cdots + \frac{1}{j\omega L_{k_0}} + j\omega C_1 + j\omega C_2 + \cdots + j\omega C_{k_1} \\
 &= \frac{1}{j\omega L_{ix}} + j\omega C_{ix},
 \end{aligned} \tag{4.20}$$

where  $L_1, L_2, \dots, L_{k_0}$  are the  $k_0$  inductances, while  $C_1, C_2, \dots, C_{k_1}$  are the  $k_1$  capacitances. They are all connected to node  $x$ .

If lossy inductances (inductance with resistance) are involved as shown in Figure 4.9,  $Y_{tx}$  becomes

$$\begin{aligned}
 Y_{tx} &= \frac{1}{j\omega L_1 + R_1} + \dots + \frac{1}{j\omega L_{k_0} + R_{k_0}} + (j\omega C_1 + G_1) + \dots + (j\omega C_{k_1} + G_{k_1}) \\
 &= \sum_{i=1}^{k_0} \frac{1}{j\omega L_i + R_i} + j\omega C_{tx} + G_{tx}.
 \end{aligned}
 \tag{4.21}$$

In such case, there is no simple express for the summation term

$$\sum_{i=1}^{k_0} \frac{1}{j\omega L_i + R_i}.
 \tag{4.22}$$

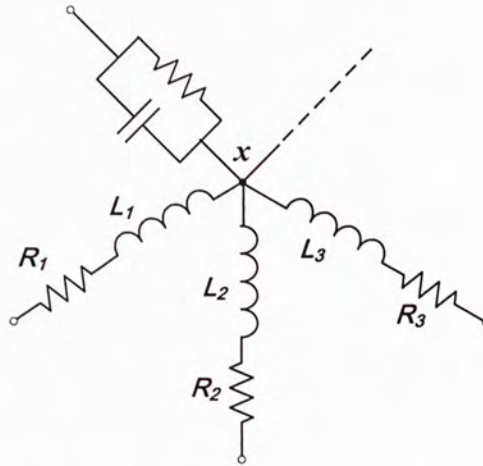


Figure 4.9 Lossy inductances connecting to node  $x$ .

As can be expected, an optimal replacement of (4.22) is in the form of

$$\frac{1}{j\omega L_{tx} + R_{tx}}.
 \tag{4.23}$$

A reasonable way to find  $L_{tx}$  and  $R_{tx}$  is to match the moments [25] of the two expressions in (4.22) and (4.23).

Expand (4.23) into power series, we get

$$\frac{1}{j\omega L_{tx} + R_{tx}} = (j\omega)^{-1} \frac{1}{L_{tx}} - (j\omega)^{-2} \frac{R_{tx}}{L_{tx}^2} + (j\omega)^{-3} \frac{R_{tx}^2}{L_{tx}^3} + \dots \quad (4.24)$$

Similarly, if expanding (4.22) into power series, we get

$$\sum_{i=1}^{k_0} \frac{1}{j\omega L_i + R_i} = (j\omega)^{-1} \sum_{i=1}^{k_0} \frac{1}{L_i} - (j\omega)^{-2} \sum_{i=1}^{k_0} \frac{R_i}{L_i^2} + (j\omega)^{-3} \sum_{i=1}^{k_0} \frac{R_i^2}{L_i^3} + \dots \quad (4.25)$$

Equating the first two moments (coefficients of the  $(j\omega)^{-1}$  and  $(j\omega)^{-2}$  terms) of (4.24) and (4.25), respectively, we can solve for  $R_{tx}$  and  $L_{tx}$ :

$$L_{tx} = \left( \sum_{i=1}^{k_0} \frac{1}{L_i} \right)^{-1}, \quad (4.26)$$

$$R_{tx} = \left( \sum_{i=1}^{k_0} \frac{1}{L_i} \right)^{-2} \sum_{i=1}^{k_0} \frac{R_i}{L_i^2}. \quad (4.27)$$

The above approximation and combination are illustrated in Figure 4.10.

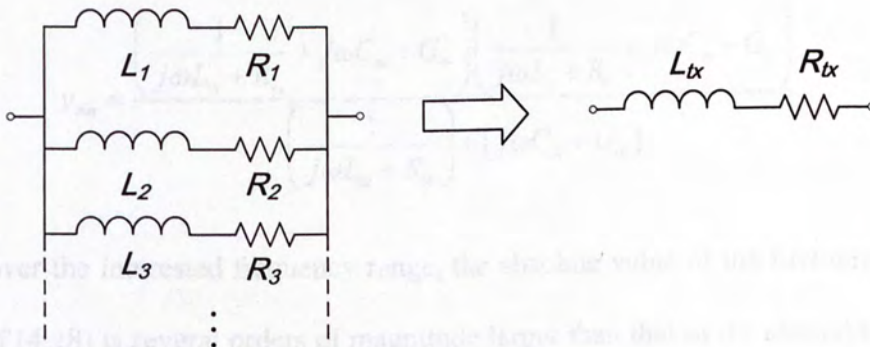


Figure 4.10 Combination of lossy inductances.

It should be noted equation (4.26) and (4.27) gives excellent approximation to (4.22) at high frequency range. After combination, the lossy inductances in (4.23) brings in error, but the following MOR process can be done recursively.

#### 4.5.1.3 Criterion for Choosing the Target Node

Not all nodes have the same impact on the whole circuit, that is, the circuit may be sensitive to some nodes, but less sensitive to some others. If we can find and eliminate the node that is least important to the network each cycle of reduction (we eliminate one node each time), the reduced circuit must have preserved the features close to the unreduced. Thus for different reduction schemes, different criteria for choosing the target node may be applied to achieve the best effect.

In [22], the circuit is treated in *RC* part and *LC* part separately, and one of the *RC* or *LC* node time constants is chosen as the criterion. But in this work, *RLC* components are considered altogether, hence the node-choosing criterion is different.

Since  $y_m$ ,  $y_n$  and  $Y_{tx}$  are now all combinations of basic components,  $y_{mn}$  in equation (4.19) can be specifically written out:

$$y_{mn} = \frac{\left( \frac{1}{j\omega L_m + R_m} + j\omega C_m + G_m \right) \left( \frac{1}{j\omega L_n + R_n} + j\omega C_n + G_n \right)}{\left( \frac{1}{j\omega L_{tx} + R_{tx}} \right) + (j\omega C_{tx} + G_{tx})}. \quad (4.28)$$

Usually, over the interested frequency range, the absolute value of the first term in the denominator of (4.28) is several orders of magnitude larger than that of the second term. Therefore we define

$$gap = \left| \frac{1}{\sqrt{(L_{ix} + R_{ix} / j\omega_0)(C_{ix} + G_{ix} / j\omega_0)}} \right| \quad (4.29)$$

as our criterion constant, where  $\omega_0$  is a selected frequency within the frequency range of interest. This constant  $gap$  can be easily understood: if degrading the lossy components to their lossless forms, equation (4.29) gives exactly the node's equivalent  $LC$  tank's resonance frequency, which indicates on which frequency scope the node may have significant impact. Hence the larger the deviation from this value to the interested frequency range, the less critical it is to the whole circuit. Consequently, the node with the largest  $gap$  is our target node to be removed.

Furthermore, a predefined value  $gap_{min}$  should be given to  $gap$  as a stop criterion for the reduction process. That is to say, once no nodes'  $gap$  exceeds  $gap_{min}$ , the whole reduction process will cease. This  $gap_{min}$  value depends on the highest frequency of interest  $f_{max}$ , and the value  $10f_{max}$  is found satisfactory through numerical experiments.

It is always a tradeoff between the complexity of the resultant circuit and the accuracy.

#### 4.5.1.4 Different Expansion Cases

Theoretically, by expanding  $y_{mn}$  in power series and retaining the first several moments, the corresponding components can be found systematically. For example, in Laplacian domain:

$$y_{mn} = m_{-1}s^{-1} + m_0s^0 + m_1s^1 + m_2s^2 + \dots, \quad (4.30)$$

where  $m_{-1}$  stands for the susceptance (reciprocal of inductance),  $m_0$  means the resistance and  $m_1$  is the capacitance. However, if expanding (4.28) directly, the resultant terms will be complicated and excessive, which is unpractical to make any decisions on their approximations.

Accordingly, we consider different combinations of  $y_m$  and  $y_n$  individually and then make approximation to  $y_{mn}$ . Besides, when performing Taylor expansion, the term  $(j\omega C_{tx} + G_{tx})$  in the denominator of (4.28) will be neglected, because the node selected to be eliminated always make it much smaller than other terms; further this can save much computer time during the Taylor expansion period.

Due to the fact that  $y_m$  or  $y_n$  can either be lossy capacitance or lossy inductance, there are three possible combination cases:

**(1). Lossy Inductance  $y_m$  and Lossy Inductance  $y_n$**

Under this occasion,  $y_m = j\omega C_m + G_m$  and  $y_n = j\omega C_n + G_n$ , thus the adjoining admittance becomes

$$y_{mn} = \frac{(j\omega C_m + G_m)(j\omega C_n + G_n)}{j\omega L_{tx} + R_{tx}}. \quad (4.31)$$

Expand (4.31), we get

$$y_{mn} = R_{tx} G_m G_n + j\omega (R_{tx} C_n G_m + R_{tx} C_m G_n + L_{tx} G_m G_n) + \dots. \quad (4.32)$$

Therefore the new components obtained are capacitance  $C_{mn}$  in parallel with conductance  $G_{mn}$ :

$$\begin{cases} C_{mn} = R_{tx} C_n G_m + R_{tx} C_m G_n + L_{tx} G_m G_n \\ G_{mn} = R_{tx} G_m G_n \end{cases}. \quad (4.33)$$

**(2). Lossy Inductance  $y_m$  and Lossy Inductance  $y_n$**



Under this occasion,  $y_m = \frac{1}{j\omega L_m + R_m}$  and  $y_n = \frac{1}{j\omega L_n + R_n}$ , thus the adjoining admittance becomes

$$y_{mn} = \frac{\left(\frac{1}{j\omega L_m + R_m}\right)\left(\frac{1}{j\omega L_n + R_n}\right)}{\frac{1}{j\omega L_{tx} + R_{tx}}}. \quad (4.34)$$

Expand (4.34), we get

$$y_{mn} = (j\omega)^{-1} \frac{L_{tx}}{L_m L_n} + (j\omega)^{-2} \left( \frac{R_{tx}}{L_m L_n} - \frac{L_{tx} R_m}{L_m^2 L_n} - \frac{L_{tx} R_n}{L_n^2 L_m} \right) + \dots. \quad (4.35)$$

By matching the first two moments of (4.35) and a power series of lossy inductance as in (4.24) of section 4.5.1.2, we can find the new lossy components are inductance  $L_{mn}$  in series with a resistance  $R_{mn}$ :

$$\begin{cases} L_{mn} = \frac{L_m L_n}{L_{tx}} \\ R_{mn} = \frac{L_n R_m}{L_{tx}} + \frac{L_m R_n}{L_{tx}} - \frac{L_m L_n R_{tx}}{L_{tx}^2} \end{cases}. \quad (4.36)$$

### (3). Lossy Capacitance $y_m$ and Lossy Inductance $y_n$

For this case,  $y_m = j\omega C_m + G_m$  and  $y_n = \frac{1}{j\omega L_n + R_n}$ , thus the adjoining admittance becomes

$$y_{mn} = \frac{(j\omega C_m + G_m)\left(\frac{1}{j\omega L_n + R_n}\right)}{\frac{1}{j\omega L_{tx} + R_{tx}}}. \quad (4.37)$$

Expand (4.37), we get

$$\begin{aligned}
 y_{mn} = j\omega \frac{C_m L_{tx}}{L_n} + (j\omega)^0 \left( \frac{G_m L_{tx}}{L_n} + \dots \right) + \\
 (j\omega)^{-1} \left( \frac{G_m R_{tx}}{L_n} + \dots \right) + (j\omega)^{-2} \left( -\frac{R_{tx} G_m R_n}{L_n^2} + \dots \right) + \dots,
 \end{aligned} \tag{4.38}$$

where the higher order terms are omitted.

Similarly, we can find that the obtained new components are a lossy capacitance in shunt with a lossy inductance:

$$\begin{cases} C_{mn} = \frac{C_m L_{tx}}{L_n}, & G_{mn} = \frac{G_m L_{tx}}{L_n} \\ L_{mn} = \frac{L_n}{G_m R_{tx}}, & R_{mn} = \frac{R_n}{G_m R_{tx}} \end{cases} \tag{4.39}$$

With all possible cases considered, each adjoining admittance now has turned into basic components, and then the reduction process can move on to the next targeted node.

#### 4.5.1.5 Type I MOR Examples

Even though Type I MOR technique is not a very efficient scheme (see the discussion subsection), we still give two examples to show the performance of the scheme.

##### (1). A simple network matching design for power amplifier output

The shape of this design is shown in Figure 4.11, where the dimension of the dielectric box is  $3.94\text{mm} \times 2.69\text{mm} \times 1\text{mm}$ , and the width for microstrip is  $0.15\text{mm}$ . The metal strip is made of copper with a finite conductivity of  $5.8 \times 10^7 \text{ S}\cdot\text{m}^{-1}$ , and the relative permittivity for the dielectric is 9.1 with a loss tangent equals 0.008.

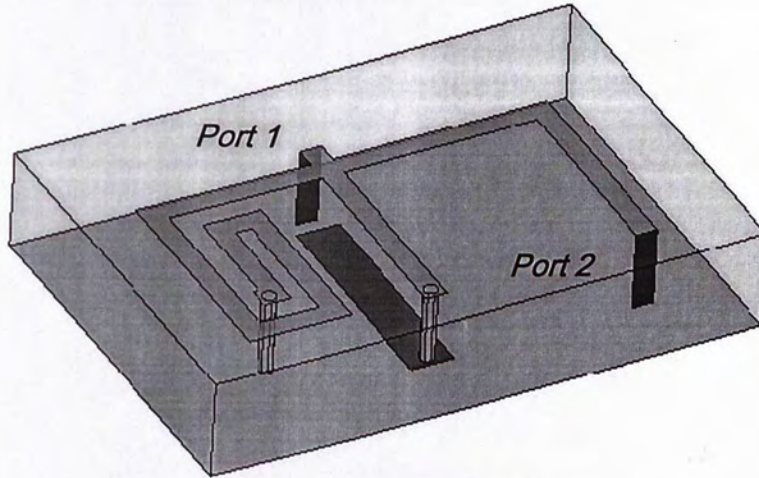


Figure 4.11 PA output matching network.

The working frequency ranges from 1.5GHz to 3.5GHz. A total 30 nodes' network is extracted originally, and all the resistances are generated at the highest working frequency condition (3.5GHz). After performing the Type I MOR, a concise circuit model (with only 4 nodes left) is obtained. If ignoring the negative elements, the S-parameters can be plotted in Figure 4.12. Besides, the curves from the reduced model, the original PEEC model and those from a commercial full-wave EM model are also shown in Figure 4.12 for comparison purpose.

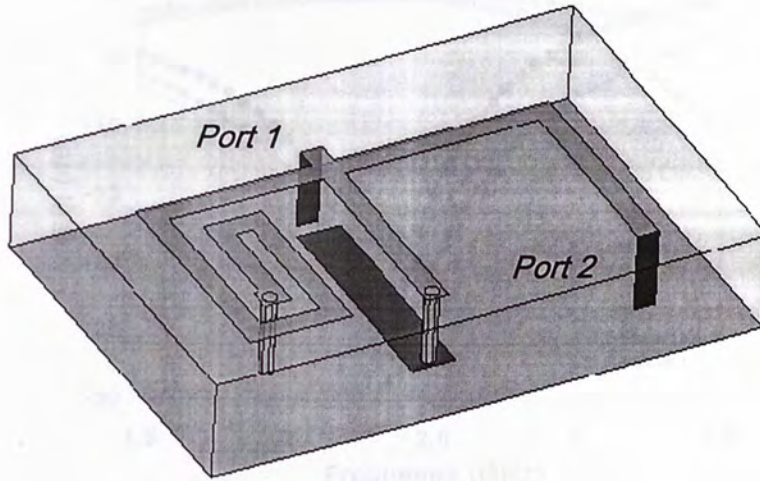
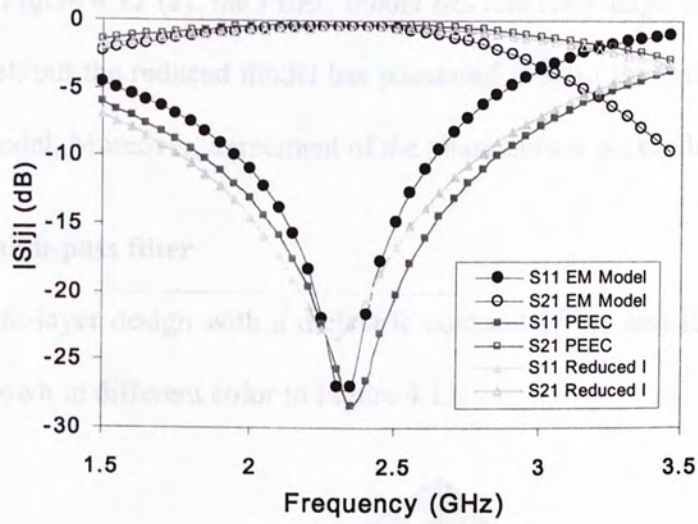
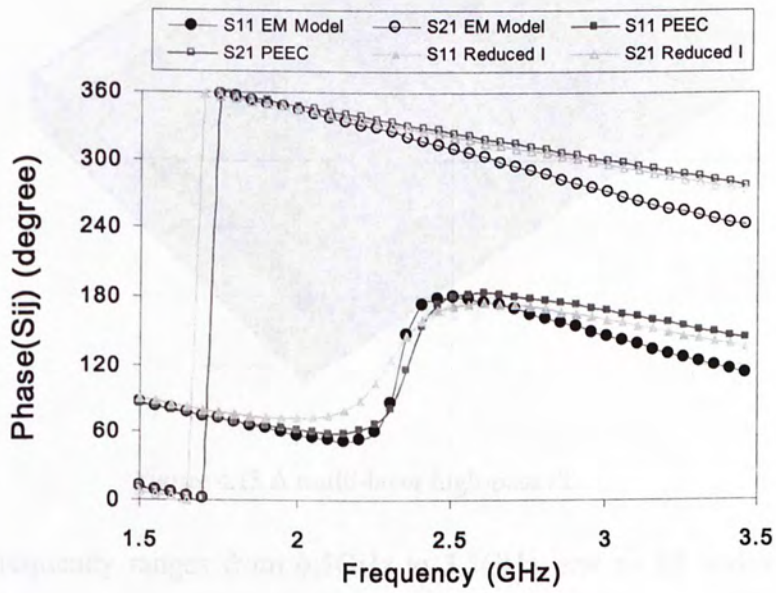


Figure 4.11 PA output matching network.

The working frequency ranges from 1.5GHz to 3.5GHz. A total 30 nodes' network is extracted originally, and all the resistances are generated at the highest working frequency condition (3.5GHz). After performing the Type I MOR, a concise circuit model (with only 4 nodes left) is obtained. If ignoring the negative elements, the S-parameters can be plotted in Figure 4.12. Besides, the curves from the reduced model, the original PEEC model and those from a commercial full-wave EM model are also shown in Figure 4.12 for comparison purpose.



(a)



(b)

Figure 4.12 S-parameters magnitude (a) and phase (b) of the EM model, PEEC model and Type I MOR reduced model of PA output network.

It can be seen in Figure 4.12 (a), the PEEC model has relatively large difference from the full-wave EM model, but the reduced model has possessed most of the information from the unreduced PEEC model. Moreover, agreement of the phase curves is excellent.

## (2). A multi-layer high-pass filter

This filter is an eight-layer design with a dielectric constant of 9.1 and loss tangent 0.008. Different layer is shown in different color in Figure 4.13.

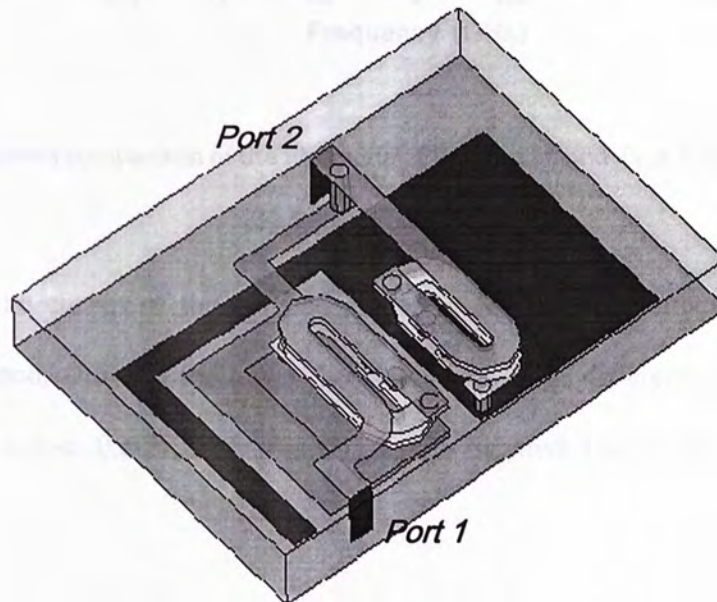


Figure 4.13 A multi-layer high-pass filter.

The working frequency ranges from 0.5GHz to 3.5GHz, and an 82 nodes network with more than 500 elements and couplings is obtained by PEEC model. After applying Type I MOR, only 17 nodes left. The S-parameters comparison is shown in Figure 4.14.

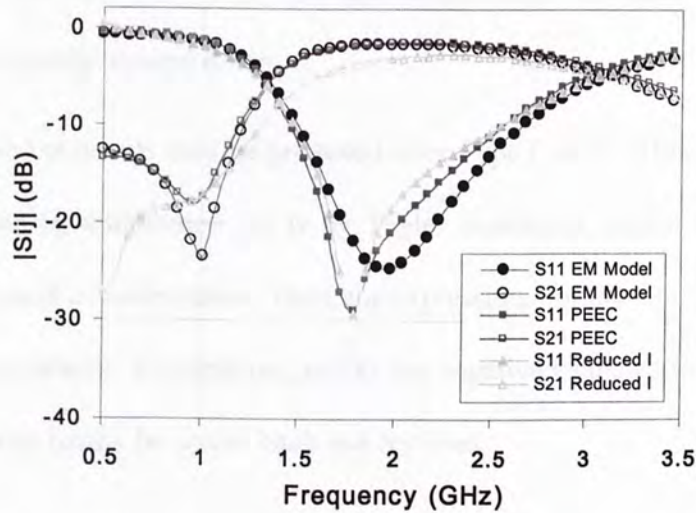


Figure 4.14 S-parameters comparison of the EM model, PEEC model and Type I MOR reduced model of a high-pass filter.

It can be seen the curves of the reduced model agrees with the unreduced better to the higher frequency end, while in the lower frequency end, large difference appears:  $S_{11}$  even becomes positive below 0.6GHz. This is due to the negative-valued components resulted from MOR.

#### 4.5.1.6 Discussion on Type I MOR

The two examples given above has demonstrated the effect of Type I MOR, however there are several drawbacks lying in this MOR:

(1). The speed of Type I MOR is not fast comparing to Type II MOR to be presented. There are two reasons for this. First, the case selection procedure for simplifying the adjoining admittances  $y_{mn}$  takes time. Second, each time before we remove a node, we need to calculate the combination of lossy inductance, i.e.  $j\omega L_{tx} + R_{tx}$  in equation (4.28). As shown in

subsection 4.5.1.2, this combination is also time-consuming. Therefore the whole Type I MOR speed is significantly slowed down.

(2). Negative-valued elements may be produced after Type I MOR. This is because simplification to the adjoining admittance  $y_{mn}$  is by Taylor expansion, which is a mathematical process lacking physical considerations. Thus, the expressions for the simplified  $y_{mn}$  can give negative values occasionally. Furthermore, unlike the negative elements in Type II MOR (to be presented), they can hardly be traced back and rectified.

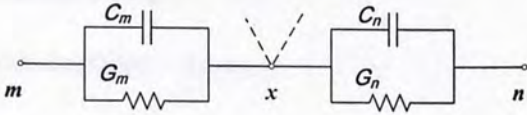
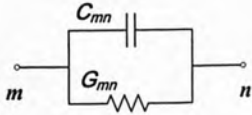
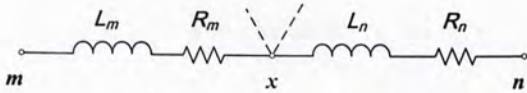
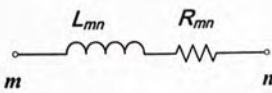
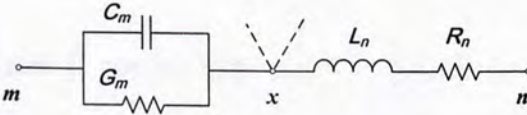
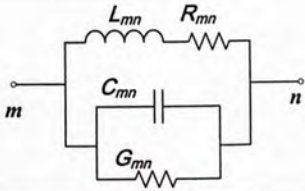
(3). The expanding point affects the accuracy of Type I MOR. Actually, the expanding point used for simplifying case 2 as shown in subsection 4.5.1.4 is infinity. Since inductances' behavior usually dominates the whole system's performance, the obtained reduced circuit model is more accurate in the higher frequency end than in the lower frequency end. This phenomenon is evident in Figure 4.14.

Despite the drawbacks, there is still room to improve this physical MOR scheme in our future work.

Table 4.1 has summarized the simplification made to the adjoining admittance in Type I MOR.



Table 4.1 Type I MOR case summary.

	$y_m$ and $y_n$	Simplified $y_{mn}$
Case 1		
Case 2		
Case 3		

## 4.5.2 Derived Complex-valued MOR Scheme (Type II)

Taylor expansion based physical MOR can convert a very large-sized circuit network into a significantly reduced yet realizable circuit. As can be seen from the examples given before, the performance of the reduced model agrees well with the unreduced one. However, the whole MOR process is time-consuming. Besides, for saving computational time, the lossy model used in Type I MOR is calculated on a fixed frequency point, which cannot actually reflect the frequency-varying property of loss for most EM layouts. Therefore a new Type II MOR scheme that is based on complex-valued electrical components is brought up.

### 4.5.2.1 The Concept of Complex Inductances and Capacitances

In Type I MOR, the basic electrical components are lossy inductances and lossy capacitances as shown in Figure 4.8, where each basic lossy component is actually composed by two com-

ponents. However, when in Type II MOR, we use one complex-valued electrical component to express the lossy inductance or loss capacitance. The real part of the complex value stands for the capacitance (inductance), while the imaginary part is used to express the lossy element, i.e. conductance (resistance). The transformation to complex-valued component is shown below:

$$Y_L = \frac{1}{j\omega L + R_L} = \frac{1}{j\omega(L + R_L / j\omega)} = \frac{1}{j\omega\tilde{L}}; \quad (4.40)$$

$$Y_C = j\omega C + G_C = j\omega(C + G_C / j\omega) = j\omega\tilde{C}, \quad (4.41)$$

in which  $\tilde{L}$  and  $\tilde{C}$  are the new basic components, and “ $\sim$ ” denotes they are complex numbers. Obviously, both  $\tilde{L}$  and  $\tilde{C}$  are frequency dependent, implying a necessity of circuit reduction at all frequency points.

Similarly, in order to continuously perform the Type II MOR, we need to simplify the adjoining admittance  $y_{mn}$ , so as to make sure it is compatible with the basic complex electrical components.

#### 4.5.2.2 Principle of Type II MOR Scheme

The idea of this scheme is originated from [5] by Wang Jie et al., but in [5], the MOR scheme only works with lossless passives design. Here in this work, Type II MOR has been extended to lossy situations, with complex-valued components introduced.

Substituting in the updated basic components, equation (4.19) becomes

$$y_{mn} = \frac{\left( \frac{1}{j\omega\tilde{L}_m} + j\omega\tilde{C}_m \right) \left( \frac{1}{j\omega\tilde{L}_n} + j\omega\tilde{C}_n \right)}{\frac{1}{j\omega\tilde{L}_{tx}} + j\omega\tilde{C}_{tx}}. \quad (4.42)$$

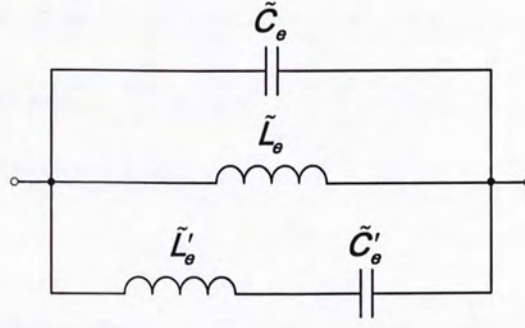
Instead of expanding it into power series and truncating the higher order terms, (4.42) is first partitioned into a partial-fractional-like form without any approximation:

$$y_{mn} = j\omega\tilde{C}_e + \frac{1}{j\omega\tilde{L}_e} + \frac{1}{j\omega\tilde{L}'_e + 1/j\omega\tilde{C}'_e}, \quad (4.43)$$

where

$$\begin{aligned} \tilde{L}_e &= \frac{\tilde{L}_m\tilde{L}_n}{\tilde{L}_{tx}}, \\ \tilde{C}_e &= \frac{\tilde{C}_m\tilde{C}_n}{\tilde{C}_{tx}}, \\ \tilde{L}'_e &= \left( \frac{\tilde{C}_n}{\tilde{L}_m\tilde{C}_{tx}} + \frac{\tilde{C}_m}{\tilde{L}_n\tilde{C}_{tx}} - \frac{\tilde{L}_{tx}}{\tilde{L}_m\tilde{L}_n} - \frac{\tilde{C}_m\tilde{C}_n}{\tilde{L}_{tx}\tilde{C}_{tx}^2} \right)^{-1}, \\ \tilde{C}'_e &= \frac{\tilde{C}_n\tilde{L}_{tx}}{\tilde{L}_m} + \frac{\tilde{C}_m\tilde{L}_{tx}}{\tilde{L}_n} - \frac{\tilde{C}_m\tilde{C}_n}{\tilde{C}_{tx}} - \frac{\tilde{L}_{tx}^2\tilde{C}_{tx}}{\tilde{L}_m\tilde{L}_n}. \end{aligned} \quad (4.44)$$

The resultant components are two pairs of inductance and capacitance:  $\tilde{L}_e$  and  $\tilde{C}_e$  are in parallel with each other, while  $\tilde{L}'_e$  and  $\tilde{C}'_e$  are in series with each other. The equivalent circuit of  $y_{mn}$  is shown in Figure 4.15.


 Figure 4.15 Equivalent circuit of  $y_{mn}$ .

The bottom branch in Figure 4.15 is apparently not in compatible with the basic components as we desired, so we have to do approximation to this branch.

The expression for this branch is

$$y_{mn}^{(3)} = \frac{1}{j\omega\tilde{L}'_e + 1/j\omega\tilde{C}'_e}. \quad (4.45)$$

Substitute values of  $\tilde{L}'_e$  and  $\tilde{C}'_e$  from (4.44) into (4.45). Doing some manipulations, we can either write out a capacitance form expression

$$y_{mn}^{(3)} = \frac{j\omega\tilde{C}'_e}{1 - \omega^2\tilde{L}'_e\tilde{C}'_e} = \frac{j\omega\tilde{C}'_e}{1 - \omega^2\tilde{L}_{ix}\tilde{C}_{ix}}, \quad (4.46)$$

or an inductance from expression

$$y_{mn}^{(3)} = \frac{1/j\omega\tilde{L}'_e}{1 - 1/(\omega^2\tilde{L}'_e\tilde{C}'_e)} = \frac{1/j\omega\tilde{L}'_e}{1 - 1/(\omega^2\tilde{L}_{ix}\tilde{C}_{ix})}. \quad (4.47)$$

If the denominator of either (4.46) or (4.47) can be turned into a constant number, then this naughty branch will become a single capacitance or a single inductance. However, for most of the nodes over the RF frequency range,  $\omega^2\tilde{L}_{ix}\tilde{C}_{ix}$  in (4.46) commonly gives a value approaching zero, thus equation (4.46) is our choice of approximation.

With this approximation choice, the node having the smallest absolute value of  $\omega_0^2 \tilde{L}_{ix} \tilde{C}_{ix}$ , where  $\omega_0$  is a fixed frequency point chosen over the frequency range of interest, will be eliminated at every reduction cycle until to a prescribed threshold value is no longer satisfied, similar to that in [5].

The theory of Type II MOR scheme is very simple, but we need to sweep the whole interested frequency range to obtain a complete response curves. The frequency dependent parts of the components are from lossy elements as illustrated in equation (4.40) and (4.41), where fortunately,  $G_C$  and  $R_L$  are all mildly frequency-varying functions. Besides, once the nodes reduction order is established on a certain frequency point, i.e. which node to be first reduced and which follows, then this order will be kept on other frequency points too. Therefore the data curves can be depicted with only a few typical frequency points sampled, and the resultant circuits at different frequency are guaranteed to share the same topology with only slightly value-changed components.

### 4.5.2.3 Condition of Stability

Another important issue related is the passivity of the reduced circuit model. In Type I MOR process, it is very probably produce negative-valued elements, especially negative resistances, which are unstable factors to the network. Discarding these negative elements is not a correct solution, because usually this produces uncontrolled errors. In Type II MOR, the negative resistances may also emerge. Therefore we have to find a systematic way to prevent their adverse effect on the whole network's stability.

Since the mutual capacitance has no physical difference from self-capacitance, what's more, the mutual capacitance is usually two orders smaller than the self capacitance, the

negative elements brought up by lossy capacitances are rare. Therefore we are more focusing on negative loss with inductances.

As mentioned in the previous section dealing with the mutual couplings, some of the obtained inter-inductances are negative. Although the inter-inductances can be converted back to mutual inductances, once they are involved in the simplification of the adjoining admittance, negative components can be brought in.

The expression that may produce negative components is in equation (4.43):

$$\tilde{L}_e = \frac{\tilde{L}_m \tilde{L}_n}{\tilde{L}_{tx}}, \quad (4.48)$$

where  $\tilde{L}_e$  has the contribution both from inductances  $\tilde{L}_m$  and  $\tilde{L}_n$ .

Physically, if a node is eliminated, the corresponding two inductive meshes that used to be adjacent with this node can be thought as merged into one equivalent mesh as demonstrated in Figure 4.16.

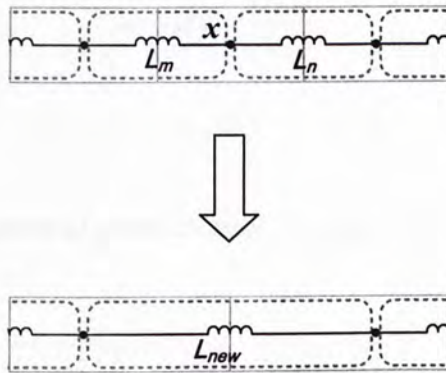


Figure 4.16 Simple illustration of equivalent inductance.

where the red dashed lines enclose the inductive meshes, and the solid grey rectangles with nodes on the centers are the capacitive meshes. The loss is always with the main inductance,

which is related to the corresponding inductive mesh. If  $L_m$  and  $L_n$  are both main inductances as shown in Figure 4.16, after node  $x$  being reduced, loss effect must be passed to the new inductance, which should still be a main inductance. Therefore in equation (4.48), if both  $\tilde{L}_m$  and  $\tilde{L}_n$  are main inductances,  $\tilde{L}_e$  is also a main inductance with a lossy term. If either  $\tilde{L}_m$  or  $\tilde{L}_n$  is inter-inductance, which is derived from mutual inductance, the resultant  $\tilde{L}_e$  must also represent a inter-inductance, where no loss factor should be involved; thus the imaginary part of  $\tilde{L}_e$ , which represents loss, should be discarded. With such treatment, the physically meaningless negative loss in a passive RF design can be effectively avoided. However, we still have to justify that  $\tilde{L}_e$  has no negative lossy part, if both  $\tilde{L}_m$  and  $\tilde{L}_n$  are main inductances.

From equation (4.40) we can write the complex inductance into exponential form:

$$\tilde{L} = L - j \frac{R_L}{\omega} = |\tilde{L}| e^{-j\alpha}, \quad (4.49)$$

where

$$\alpha = \tan^{-1} \frac{R_L / \omega}{L}, \quad (4.50)$$

and  $0 < \alpha < \pi / 2$ .

Since  $\tilde{L}_t$  is the total inductance of those connect to node  $x$ , it can be expressed as

$$\tilde{L}_t = \frac{1}{1/\tilde{L}_1 + 1/\tilde{L}_2 + \dots + 1/\tilde{L}_k} = \frac{1}{|1/\tilde{L}_1| e^{j\alpha_1} + |1/\tilde{L}_2| e^{j\alpha_2} + \dots + |1/\tilde{L}_k| e^{j\alpha_k}}, \quad (4.51)$$

where  $k$  is the total number of the inductances connecting to node  $x$ . Since commonly the inter-inductance is one or two orders larger than the main inductance, the value of  $\tilde{L}_t$  is essentially determined by the contribution of main inductors.

Express  $1/\tilde{L}_i$  in exponential form:

$$1/\tilde{L}_i = |1/\tilde{L}_i| e^{j\alpha_i}, \quad (4.52)$$

where  $\alpha_i$  is the angle of the sum vector. With the parallelogram rule for vector addition, the resultant vector  $1/\tilde{L}_i$  is shown (exaggeratedly) in Figure 4.17. Commonly the imaginary part of the inductance is commonly at least one order less than its real part. In the beginning,  $\alpha_i$  must be positive.

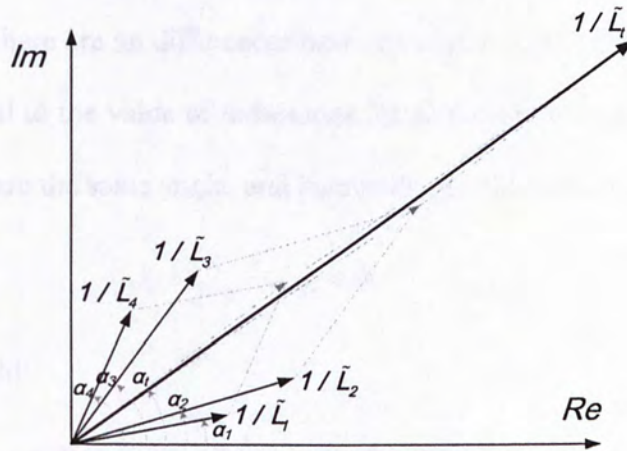


Figure 4.17 Vector representation of  $\tilde{L}_i$ .

Assuming  $\alpha_{\min}$  and  $\alpha_{\max}$  are the smallest and largest angles among  $\alpha_1, \alpha_2, \dots, \alpha_k$ , respectively, aided by Figure 4.17 we have:

$$\alpha_{\min} < \alpha_i < \alpha_{\max}. \quad (4.53)$$

Since  $\tilde{L}_e$  in equation (4.48) can be expressed like

$$\tilde{L}_e = |\tilde{L}_e| e^{j\alpha_e} = \frac{|\tilde{L}_n \tilde{L}_m|}{|\tilde{L}_i|} e^{j(-\alpha_m - \alpha_n + \alpha_i)}, \quad (4.54)$$

considering equation (4.53), angle  $\alpha_e$  can be rewritten as



$$\begin{aligned}
 \alpha_e &= -\alpha_m - \alpha_n + \alpha_t \\
 &< -\alpha_m - \alpha_n + \alpha_{\max} \\
 &= -(\alpha_{\max} - \Delta_m) - (\alpha_{\max} - \Delta_n) + \alpha_{\max} \\
 &= \Delta_m + \Delta_n - \alpha_{\max},
 \end{aligned} \tag{4.55}$$

where  $\Delta_m$  and  $\Delta_n$  are the differences of  $\alpha_m$  and  $\alpha_n$  from  $\alpha_{\max}$ , respectively. As long as

$$\Delta_m + \Delta_n - \alpha_{\max} < 0, \tag{4.56}$$

i.e.  $\alpha_e < 0$ , then there will be no negative resistances generated from  $\tilde{L}_e$  in equation (4.48).

An optimal case is there are no differences between angles of the complex inductances, i.e. the loss is proportional to the value of inductance for all complex inductances, then all main inductance vectors share the same angle, and inequality (4.56) becomes

$$-\alpha_{\max} < 0, \tag{4.57}$$

which is obviously held.

It is known that the conductor loss of a rectangular inductive cell is proportional to the aspect ratio  $l/w$ , where  $l$  is the length and  $w$  is the width of the cell (see equation (4.14)). Figure 4.18 is the plot of typical inductance value vs. the change of the inductive cell's aspect ratio. Three different colored curves represent three meshes with different length  $l$ . We observe that if the mesh length is longer (pink colored curve), the inductance is closer to proportional to the aspect ratio, hence the angle difference  $\Delta_m$  and  $\Delta_n$  are approaching zero. If the mesh length is short (blue colored curve), the slope of the curve is becoming smaller as the aspect ratio increases, in other words, the angle of the complex inductance is approaching  $\alpha_{\max}$  as the aspect ratio increases, which also makes  $\Delta_m$  and  $\Delta_n$  approach zero. We only need

to let the mesh scheme used in our PEEC model follow the above guidance, then there will be no negative resistances involved.

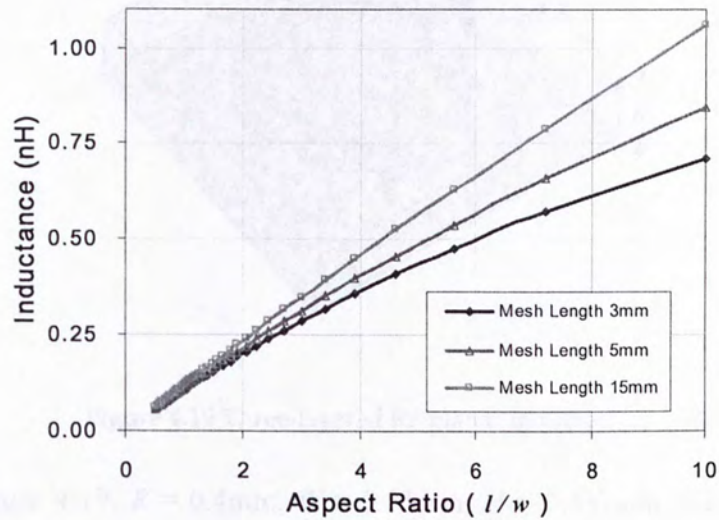


Figure 4.18 Inductance's change with the mesh shape.

#### 4.5.2.4 Type II MOR Examples

A number of examples will be given in this section to validate the proposed Type II MOR. The first example is a simple RF planar inductor and the second example is a multilayered capacitor. Other examples include a high-pass filter and a band-pass filter.

##### (1). Three-layered circular spiral RF inductor

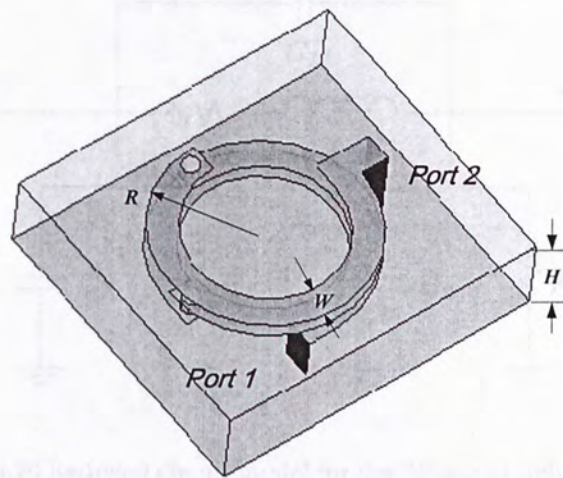


Figure 4.19 Three-layered RF planar inductor.

As shown in Figure 4.19,  $R = 0.4\text{mm}$ ,  $W = 0.15\text{mm}$ ,  $H = 0.437\text{mm}$ , the vertical distance from the ground to the first metal strip layer is  $h_0 = 0.238\text{mm}$  and the vertical gap between neighboring metal layers is  $d = 0.079\text{mm}$ . The metal strip is made by copper with a finite conductivity of  $5.8 \times 10^7 \text{ S}\cdot\text{m}^{-1}$ , and the dielectric enclosing the inductor has a relative permittivity  $\epsilon_r = 9.1$  with loss  $\tan\delta = 0.008$ .

The upper testing frequency is 5GHz, thus the original circuit extracted consists of 22 nodes with 53 lossy capacitances, 20 lossy inductances and 67 mutual couplings. After performing Type II MOR, the circuit model can be reduced to a circuit with only 3 nodes:

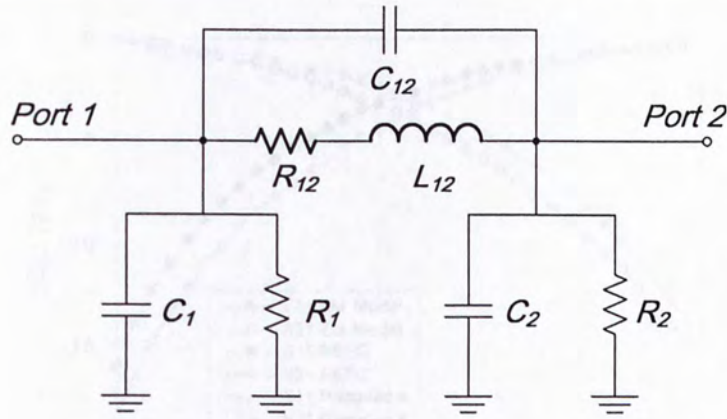


Figure 4.20 Reduced circuit model for the RF planar inductor.

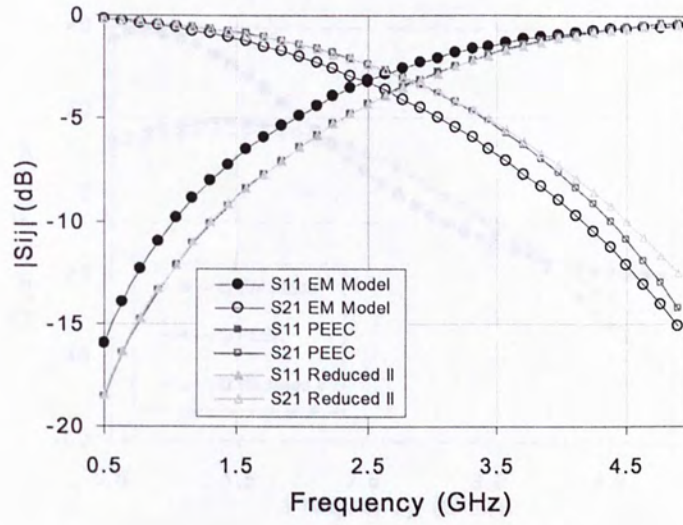
On  $f = 5\text{GHz}$ , the values of the components in Figure 4.20 are listed below:

Table 4.2 Components values for the reduced circuit of the RF planar inductor.

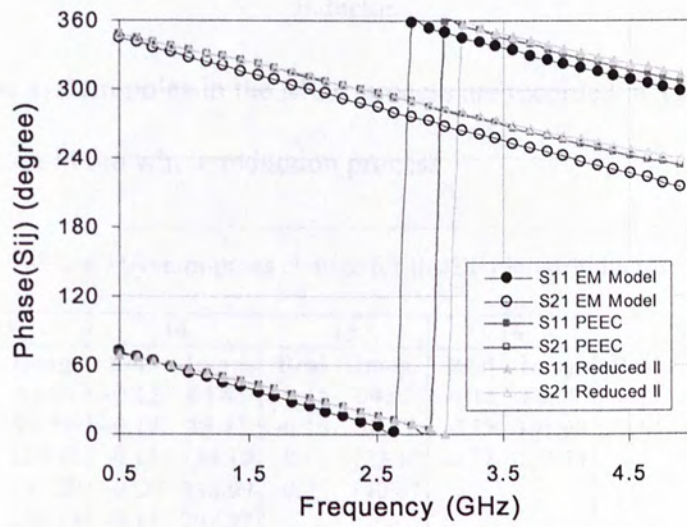
$C_1$	$0.36\text{pF}$	$R_1$	$8.95\text{k}\Omega$	$L_{12}$	$5.22\text{nH}$
$C_2$	$0.22\text{pF}$	$R_2$	$14.5\text{k}\Omega$		
$C_{12}$	$0.11\text{pF}$	$R_{12}$	$4.6\Omega$		

S-parameters comparison is shown in Figure 4.21, where the curve “EM Model” is by a FEM based commercial EM model, curve “PEEC” is for the original PEEC circuit model, and curve “Reduced II” is for Type II MOR circuit shown in Figure 4.21. The Q factors comparison is also given to show a closer view on characteristics of lossy components.

It can be observed from the figures below that the characteristics of the reduced model matches well to that of the original PEEC circuit model, as well as to that of the EM model.



(a)



(b)

Figure 4.21 S-parameters magnitude (a) and phase (b) of the EM model, PEEC model and Type II MOR model of the RF planar inductor.

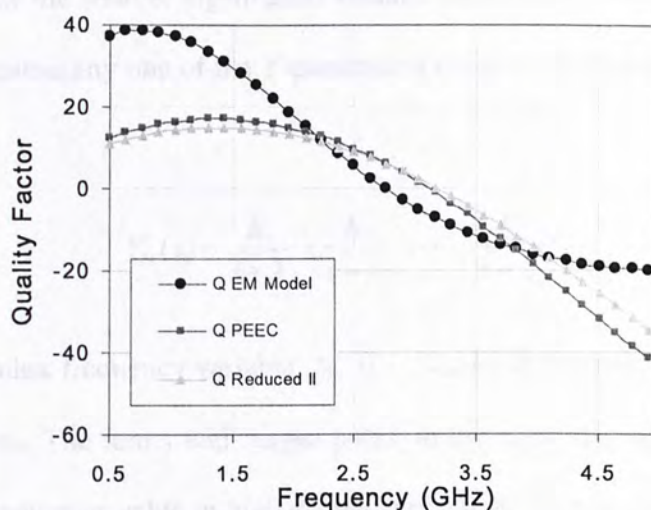


Figure 4.22 Quality factors of the EM model, PEEC model and Type II MOR model of the RF planar inductor.

The changes of the system poles in the MOR process are recorded in Table 4.3 for showing the intrinsic alternation in the whole reduction process.

Table 4.3 System poles change for the RF planar inductor.

12		13		14		15		16		17		18	
Real	Imag.	Real	Imag.	Real	Imag.	Real	Imag.	Real	Imag.	Real	Imag.	Real	Imag.
-0.14	64.52	-0.14	63.91	-0.13	64.45	-0.15	64.02	-0.14	66.69	-0.13	71.19	-0.13	72.25
-0.15	88.86	-0.17	90.56	-0.19	88.47	-0.16	89.77	-0.15	101.40	-0.14	102.51		
-0.21	122.96	-0.13	128.78	-0.14	124.10	-0.13	123.10	-0.22	153.53				
-0.21	131.53	-0.24	135.29	-0.20	138.99	-0.23	140.67						
-0.17	194.77	-0.14	238.33	-0.17	207.37								
-0.21	229.15	-0.18	198.62										
-0.10	251.77												

The numbers in the first row indicate how many nodes have been eliminated. Since at the beginning of the reduction, the poles are too many to list, we start from 12 nodes being eliminated. Table 4.3 doesn't include the negative conjugates of the above poles. Besides, all the poles shown have been normalized to  $10^{-9}$ .

It can be seen that the smaller eigenvalues remain almost unchanged as the circuit being reduced. This is because any one of the Y-parameters (such as  $Y_{21}$ ) can be written in partial fraction form like:

$$Y_{21}(s) = \frac{K_1}{s - \lambda_1} + \frac{K_2}{s - \lambda_2} + \dots + \frac{K_n}{s - \lambda_n} \quad (4.58)$$

where  $s$  is the complex frequency variable,  $\lambda_1, \lambda_2, \dots, \lambda_n$  are the system poles,  $K_1, K_2, \dots, K_n$  are constant residues. The terms with larger poles on the right side of equation (4.58) will only affect the Y-parameter value in higher frequency range, thus during MOR process they will be absorbed into other poles first.

## (2). A four-layered planar RF capacitor

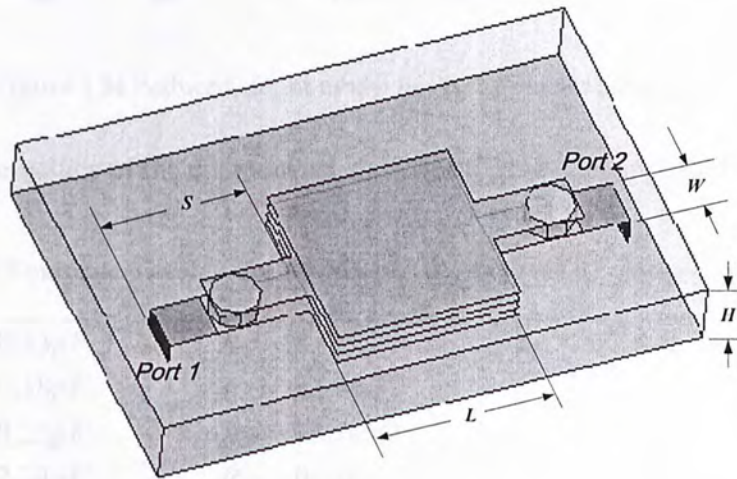


Figure 4.23 Four-layered RF planar capacitor.

As shown in Figure 4.23, the side length of the metal square is  $L = 0.762\text{mm}$ ,  $S = 0.584\text{mm}$  and  $W = 0.203\text{mm}$ . The vertical distance from the ground to the first metal strip layer is  $h_0 = 0.091\text{mm}$ , and the vertical gap between the neighboring metal layers is  $d = 0.458\text{mm}$ . The

metal strip is made by copper with a finite conductivity of  $5.8 \times 10^7 \text{ S}\cdot\text{m}^{-1}$  and the dielectric enclosing the inductor has a relative permittivity  $\epsilon_r = 7.8$  with loss  $\tan\delta = 0.01$ .

The PEEC extracted circuit has 23 nodes with 44 lossy capacitances, 22 lossy inductances and 39 mutual couplings. But it can be reduced to a simple circuit with 4 nodes left, which is shown in Figure 4.24.

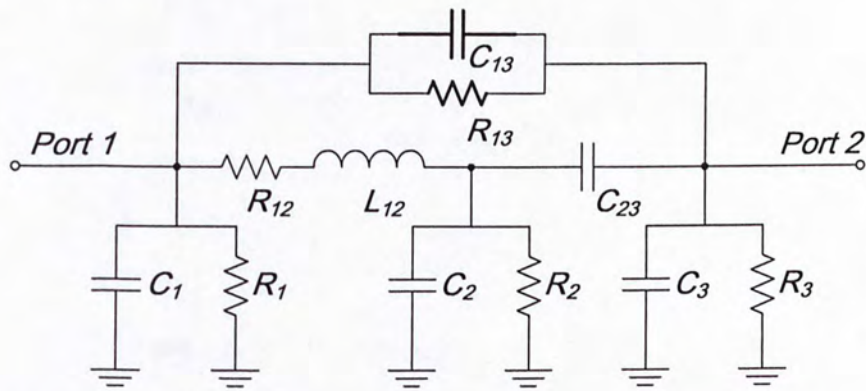


Figure 4.24 Reduced circuit model for the RF planar capacitor.

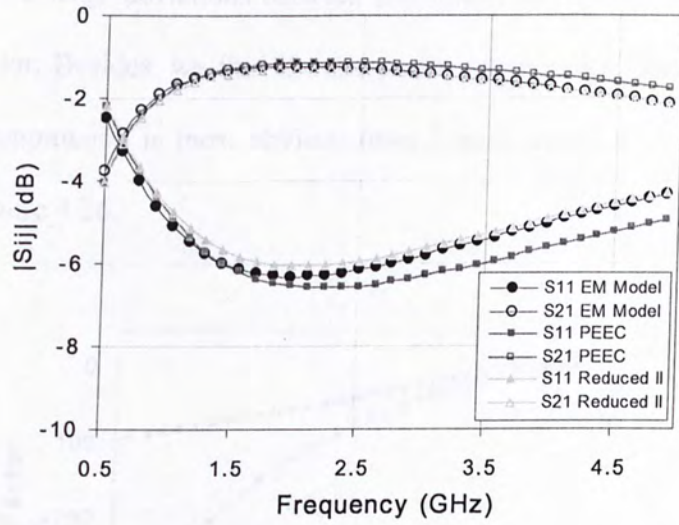
On  $f = 5\text{GHz}$ , the values of the components shown in Figure 4.24 are listed below:

Table 4.4 Components values for the reduced circuit of the RF planar capacitor.

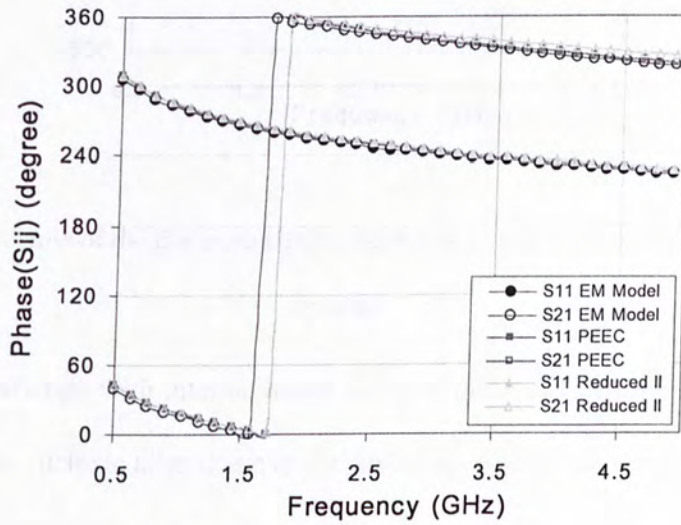
$C_1$	$0.33\text{pF}$	$R_1$	$8.96\text{k}\Omega$	$L_{12}$	$0.33\text{nH}$
$C_2$	$0.38\text{pF}$	$R_2$	$8.99\text{k}\Omega$		
$C_3$	$0.23\text{pF}$	$R_3$	$13.70\text{k}\Omega$		
$C_{13}$	$2.34\text{pF}$	$R_{12}$	$0.16\Omega$		
$C_{23}$	$0.38\text{pF}$	$R_{13}$	$14.52\text{k}\Omega$		

S-parameters comparison is shown in Figure 4.25:





(a)



(b)

Figure 4.25 S-parameters magnitude (a) and phase (b) of the EM model, PEEC model and Type II MOR model of the RF planar capacitor.

Clearly, the reduced model has achieved satisfactory result. Further, Q factors comparison is plotted in Figure 4.26, where curve from reduced model with 5 nodes left is also potted. It

can be seen there are large deviations between EM model and PEEC models; however the curve trend is similar. Besides, we find if more nodes get removed, less accurate result we will have. This phenomenon is most obvious from 5-node model to 4-node model as the curves shown in Figure 4.26.

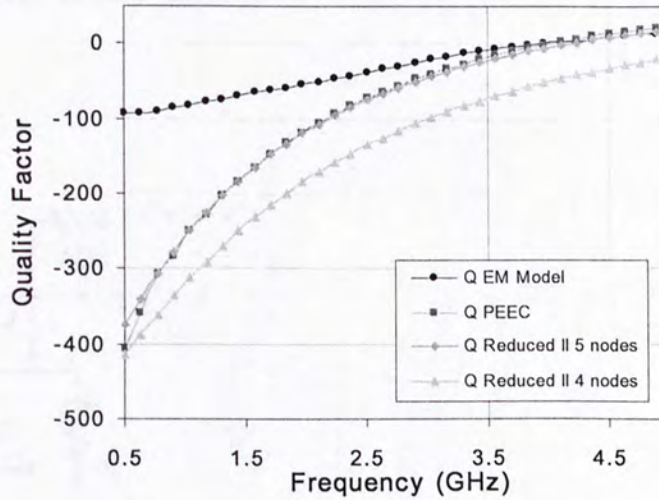


Figure 4.26 Quality factors of the EM model, PEEC model and Type II MOR model of the RF planar capacitor.

The system poles change with internal nodes being eliminated is also recorded in Table 4.5 for demonstrating the intrinsic alternation in the whole reduction process.

Table 4.5 System poles change for the RF planar capacitor.

13		14		15		16		17		18		19	
Real	Imag.	Real	Imag.	Real	Imag.	Real	Imag.	Real	Imag.	Real	Imag.	Real	Imag.
-0.23	25.38	-0.23	25.40	-0.23	25.33	-0.23	25.40	-0.23	25.65	-0.22	25.65	-0.24	33.68
-0.10	68.83	-0.10	67.60	-0.10	68.08	-0.10	68.06	-0.12	76.96	-0.22	75.80		
-0.14	98.80	-0.13	96.15	-0.13	96.04	-0.14	97.71	-0.22	92.99				
-0.16	128.68	-0.17	125.77	-0.18	124.59	-0.18	126.64						
-1.52	217.09	-0.94	255.32	-0.38	330.65								
-0.25	348.83	-0.14	370.80										
-0.12	375.60												

Similar to Table 4.4, the negative conjugates of the above poles aren't shown, and all the data are normalized to  $10^{-9}$ .

**(3). An eight-layered high-pass filter**

It is first shown in Figure 4.13, and we now perform Type II MOR on it. After MOR, the original 82-node circuit is reduced to a simple 5-node network shown below:

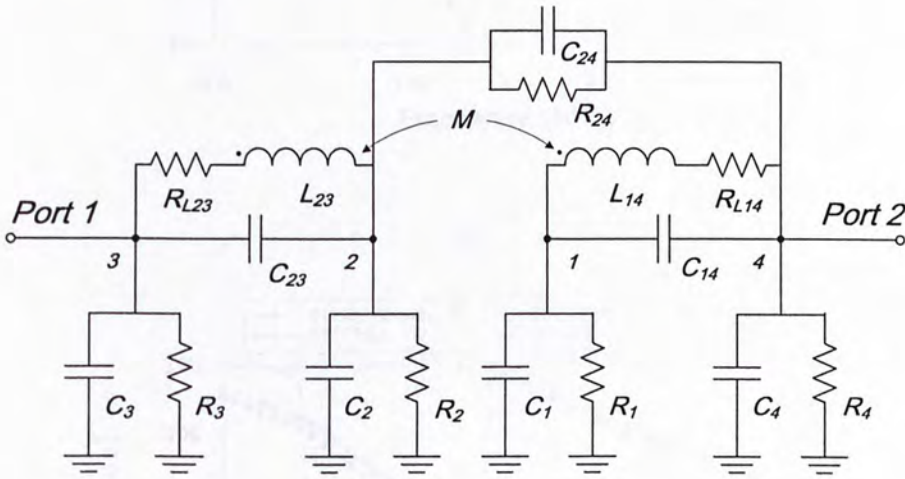


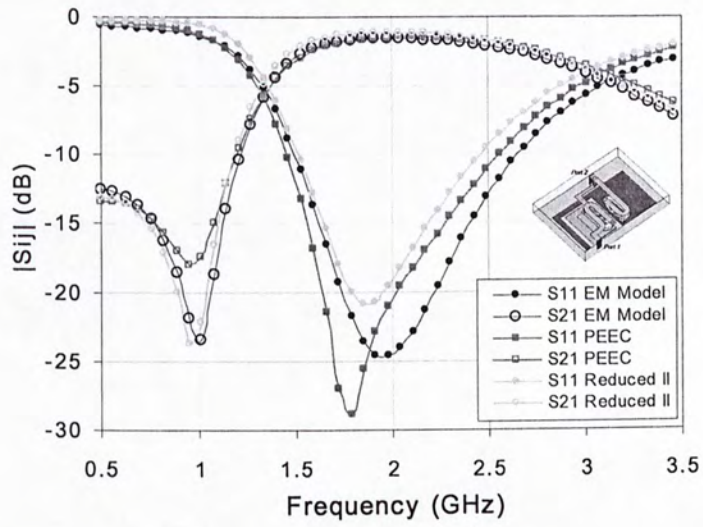
Figure 4.27 Reduced circuit model for the RF high-pass filter.

On  $f = 5\text{GHz}$ , the values of the components shown in Figure 4.27 are listed below:

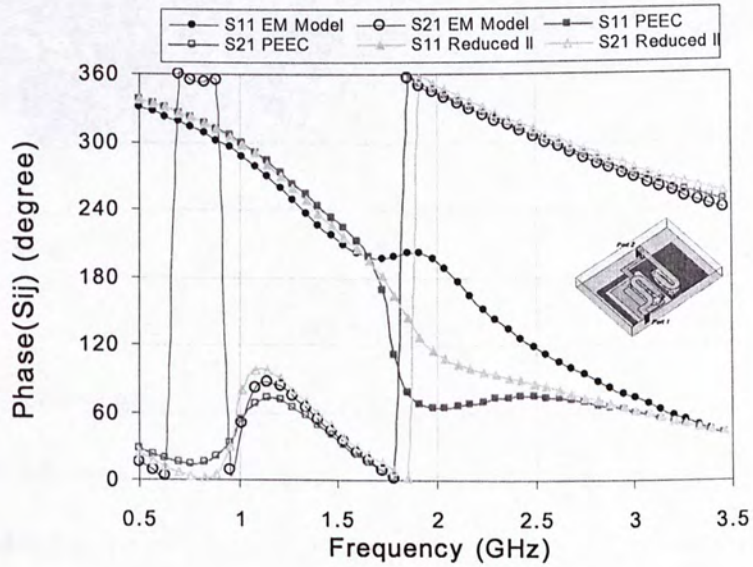
Table 4.6 Components values for the reduced circuit of RF high-pass filter.

$C_1$	$4.98\text{pF}$	$R_1$	$1.15\text{k}\Omega$	$L_{23}$	$5.28\text{nH}$
$C_2$	$63.92\text{fF}$	$R_2$	$0.13\text{M}\Omega$	$L_{14}$	$5.37\text{nH}$
$C_3$	$72.71\text{fF}$	$R_3$	$61.85\text{k}\Omega$	$M$	$83.10\text{pH}$
$C_4$	$1.33\text{pF}$	$R_4$	$4.13\text{k}\Omega$		
$C_{14}$	$0.15\text{pF}$	$R_{24}$	$0.12\text{M}\Omega$		
$C_{23}$	$0.11\text{pF}$	$R_{L23}$	$6.53\Omega$		
$C_{24}$	$1.22\text{pF}$	$R_{L14}$	$6.71\Omega$		

The S-parameters comparison is shown in Figure 4.28, where curves from traditional EM model, original PEEC model and Type II MOR model are plotted.



(a)



(b)

Figure 4.28 S-parameters magnitude (a) and phase (b) of the EM model, PEEC model and Type II MOR model of RF high-pass filter.

It can be seen after Type II MOR, the resultant 5-node circuit can perfectly represent the original physical RF layout design, since all key elements and accumulated parasitics are all included.

#### (4). A five-layer RF band-pass filter

The overall shape is shown below in Figure 4.29:

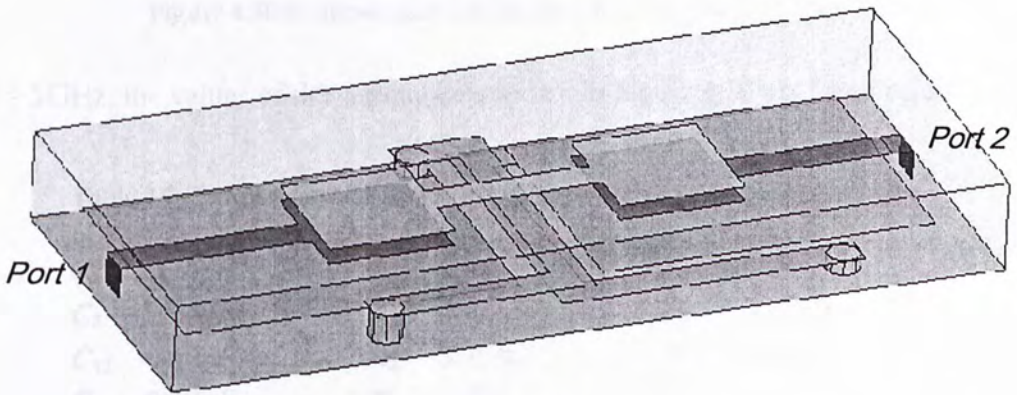


Figure 4.29 Five-layered RF band-pass filter.

The overall size is  $5.1\text{mm} \times 2.1\text{mm} \times 0.55\text{mm}$ , and the materials used are the same as those in the high-pass filter. In the beginning, circuit obtained from PEEC modeling has 183 nodes with 664 capacitance, 273 lossy inductances and 2295 mutual couplings. However, we can simplify it to a circuit with only 6 nodes:

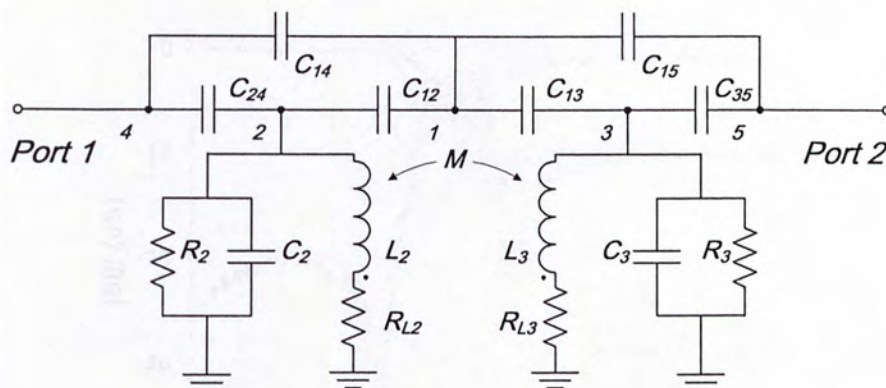


Figure 4.30 Reduced circuit model for the RF band-pass filter.

On  $f = 5\text{GHz}$ , the values of the components shown in Figure 4.30 are listed below:

Table 4.7 Components values for the reduced circuit of RF band-pass filter.

$C_2$	$2.78\text{pF}$	$R_{L2}$	$1.04\Omega$	$L_2$	$1.12\text{nH}$
$C_3$	$2.64\text{pF}$	$R_{L3}$	$1.21\Omega$	$L_3$	$1.12\text{nH}$
$C_{12}$	$0.10\text{pF}$	$R_2$	$1.13\text{k}\Omega$	$M$	$0.21\text{nH}$
$C_{13}$	$0.12\text{pF}$	$R_3$	$1.47\text{k}\Omega$		
$C_{14}$	$0.46\text{pF}$				
$C_{15}$	$0.46\text{pF}$				
$C_{24}$	$0.75\text{pF}$				
$C_{35}$	$0.74\text{pF}$				

The S-parameters comparison is shown in Figure 4.31, where curves from traditional full-wave EM model, original PEEC model and Type II MOR model are plotted.

In addition, a magnified plot of the in-band part of the curves in Figure 4.30 is also shown.

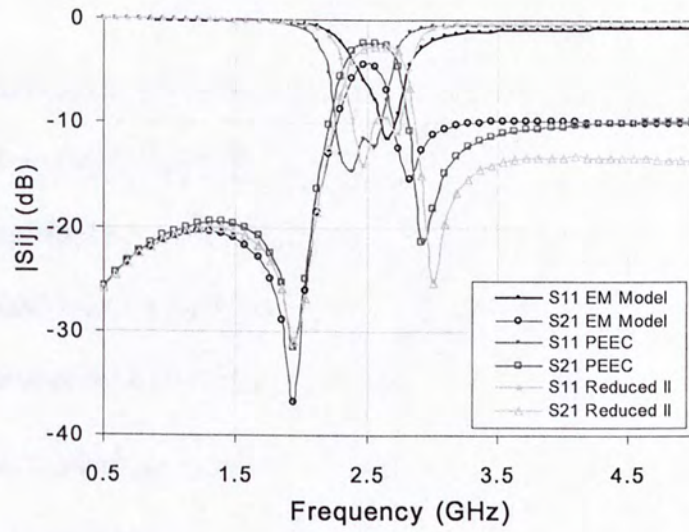


Figure 4.31 S-parameters comparison of the EM model, PEEC model and Type II MOR model of RF band-pass filter.

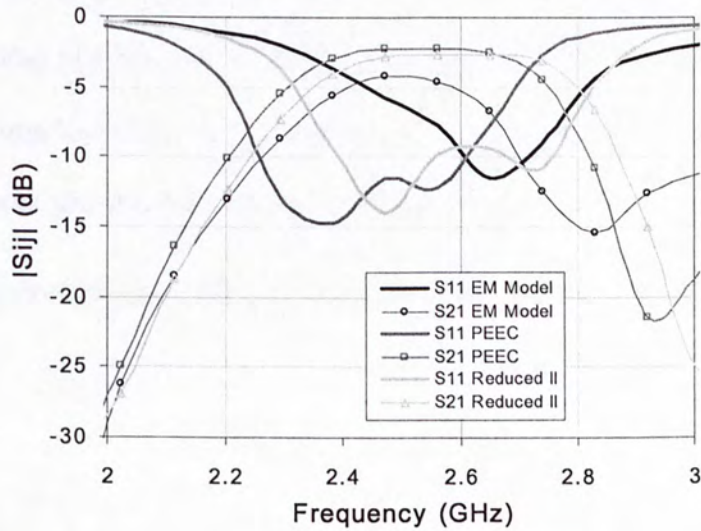


Figure 4.32 In-band plot of the curves in Figure 4.31.

Obviously, the reduced circuit model has expressed the band-pass filter design very well. With this simplified model available, modification to the RF layout can be more efficient and fast.

## 4.6 Summary

In this chapter, two types of physics-based MOR schemes are investigated. The original circuit prototype is from PEEC modeling. During MOR the key steps are the  $Y$ - $\Delta$  circuit transformation and simplification to the adjoining admittance  $y_{mn}$ . Different from mathematics-based MOR, Physical MOR simplifies the circuit topology gradually by reducing nodes and absorbing branches connecting to the target nodes.

Type I and Type II MOR all start from  $Y$ - $\Delta$  circuit transformation, but they have adopted different methods to simplify the resultant adjoining admittances to make sure the whole MOR can be recursively performed. Based on Taylor expansion, Type I MOR can give a reduced realizable circuit model. However, due to the moments matching method used to approximate the adjoining admittance, the reduction speed is relatively slow. Type II MOR first expands the adjoining admittance into three terms, each is a physically expressive equivalent circuit, and then simplifies them. In contrast, Type II MOR is more accurate and faster than Type I MOR, besides, the stability condition can be easily met.

In addition to theoretical deduction, practical examples are also given to demonstrate these two MOR schemes.

## References

- [1] K. -L. Wu, “*MAP user’s manual*”, the Chinese University of Hong Kong, Mar. 2002, Release 2.1.
- [2] P. L. Werner et al., “Extraction of SPICE-type equivalent circuits of microwave components and discontinuities using the genetic algorithm optimization technique,” *IEEE Trans. Adv. Packag.* vol. 23, pp. 55-61, Feb. 2000.



- [3] Y. Cao et al., "Frequency-independent equivalent-circuit model for on-chip spiral inductors," *IEEE J. Solid-State Circuits*, vol. 38, pp. 419-426, Mar. 2003.
- [4] J. R. Long and M. A. Copeland, "The modeling, characterization, and design of monolithic inductors for silicon RF IC's," *IEEE J. Solid-State*, vol. 32, pp. 357-369, Mar. 1997.
- [5] J. Wang and K.-L. Wu, "A derived physically expressive circuit model for multilayer RF embedded passives," *IEEE Trans. Microwave Theory Tech.*, vol. 54, pp. 1961-1968, May 2006.
- [6] B. N. Sheehan, "Branch merge reduction of RLCM networks," in *Proc. Int. Conf. on Computer Aided Design (ICCAD)*, 2003, pp. 658-664.
- [7] D. C. Lay, "*Linear Algebra and Its Applications*," Reading, Mass.: Addison-Wesley, 1997, ch.1.
- [8] D. K. Cheng, "*Field and Wave Electromagnetics*," Reading, Mass.: Addison-Wesley, 1989, ch.5.
- [9] K. B. Ashby et al., "High Q inductors for wireless applications in a complementary silicon bipolar process," *IEEE J. Solid-State*, vol. 31, pp. 4-9, Jan. 1996.
- [10] C. P. Yue and S. S. Wong, "Physical modeling of spiral inductors on silicon," *IEEE Trans. Electron Devices*, vol. 47, pp. 560-568, Mar. 2000.
- [11] C. B. Sia et al., "Physical layout design optimization of integrated spiral inductors for silicon-based RFIC applications," *IEEE Trans. Electron Devices*, vol. 52, pp. 2559-2567, Dec. 2005.

- [12] J. M. López-Villegas, J. Samitier, C. Cané, P. Losantos and J. Bausells, "Improvement of the quality factor of RF integrated inductors by layout optimization," *IEEE Trans. Microwave Theory Tech.*, vol. 48, pp. 76-83, Jan. 2000.
- [13] Z. Qin and C. K. Cheng, "Realizable parasitic reduction using Generalized Y- $\Delta$  transformation", in *Proc. 40th DAC*, June, 2003, pp. 220-225.
- [14] J. C. Rautio, "An investigation of microstrip conductor loss," *IEEE Microwave Magazine*, pp. 60-67, Dec. 2000.
- [15] R. A. Pucel, D. J. Massé, and C. P. Hartwig, "Losses in microstrip," *IEEE Trans. Microwave Theory Tech.*, vol. 16, pp. 342-350, June 1968.
- [16] R. Faraji-Dana and Y. L. Chow, "The current distribution and AC resistance of a microstrip structure," *IEEE Trans. Microwave Theory Tech.*, vol. 38, pp. 1268-1277, Sept. 1990.
- [17] M. Kobayashi and H. Sekine, "Closed-form expressions for the current distribution on open microstrip lines," *IEEE Trans. Microwave Theory Tech.*, vol. 39, pp.1115-1119, July 1991.
- [18] E. J. Denlinger, "Losses of microstrip lines," *IEEE Trans. Microwave Theory Tech.*, vol. MTT-28, pp. 513-522, June 1980.
- [19] W. T. Weeks, L. L. Wu, M. F. McAllister and A. Singh, "Resistive and inductive skin effect in rectangular conductors," *IBM J. Res. Develop.*, vol. 23, pp. 652-660, Nov. 1979.
- [20] N. A. Talwalker, C. P. Yue and S. S. Wong, "Analysis and synthesis of on-chip spiral inductors," *IEEE Trans. Electron Devices*, vol. 52, pp. 176-182, Feb. 2005.

- [21] K. M. Coperich, A. E. Ruehli and A. Cangellaris, "Enhanced skin effect for partial-element-equivalent-circuit (PEEC) models," *IEEE Trans. Microwave Theory Tech.*, vol. 48, pp. 1435-1442, Sept. 2000.
- [22] C. S. Amin et al., "Realizable reduction of inter-connect circuits including self and mutual inductances," *IEEE Trans. Computer-Aided Design*, vol. 24, pp. 271-277, Feb. 2005.
- [23] B. N. Sheehan, "TICER: realizable reduction of extracted RC circuits," in *Proc. Int. Conf. Computer-Aided Design*, 1999, pp. 200-203.
- [24] P. J. H. Elias and N. P. van der Meijs, "Efficient moments extraction of large inductively coupled interconnection network," in *Proc. Int. Symp. Circuits Syst.*, 1996, pp. IV 540-IV 543.
- [25] R. F. Harrington, "*Field Computation by Moment Methods*," New York: Macmillan, 1993, ch.1.

## Chapter 5

### CONCLUDING REMARKS

#### 5.1 Conclusion

This thesis has investigated two different categories of MOR schemes, both of which aim to simplify the circuit model obtained from PEEC modeling.

In order to facilitate our LTCC designs in CUHK here, we have been advancing PEEC modeling technique for years. So far our PEEC algorithm is capable of dealing with various types of planar structures and via holes in 2.5D RF layouts. Quasi-static approximation is employed for saving computing time. Although the original intention to use PEEC is to model low-loss passive RF products, in this thesis we have enabled it to handle lossy cases by superimposing reasonably calculated loss models.

Different from other EM solvers, PEEC generates an equivalent circuit network representing the features of the original RF layout. Feeding the obtained circuit into proper circuit solver, we can perform both time domain and frequency domain analysis. Once having grasped the circuit domain behavior, the designers can be more easily fine tune their designs. However, if higher accuracy is required, then more complicated the obtained circuit will become. Therefore, MOR must be performed before advancing other processes.

Mathematical MOR can reduce a large model to a small model; however, the reduction is performed in pure mathematics realms, where little physical aspects of the circuit need to be considered. Hence it is merely focusing on how to preserve a less distorted input-output behavior from the original model.

Physical MOR starts from the Gaussian elimination method, during which the internal circuit nodes are eliminated one by one, and the attached lumped elements are being gradually absorbed into their neighbor branches following certain rules. In the end, circuit in a very small scale can be achieved. Physical MOR concerns more about the overall electronic features of the circuit and only eliminates those nodes least critical to the entire network, thus most of the physical property in the reduced model is preserved from the original model as expected.

This thesis has given both the theories and examples to both of the above two MOR schemes. Generally speaking, mathematical MOR works faster and the data curves gained are more optimal, while the physical MOR works slightly slower but gives back a fully reduced circuit topology. Besides, the theory of mathematical MOR is abstruse, while the physical MOR is very simple. In chapter 4, two physical MOR schemes that can deal with lossy models are introduced, where Type II MOR is more favored, since it works faster and is easier to implement.

## **5.2 Future Improvement**

The accuracy of the lossy model affects the MOR results achieved; therefore to build a more practical model that reflects real situations can be one of the future aims.

Another factor affects the lossy model's calculation and application is the meshing scheme. Rectangular or circular shaped meshing cells are enough for a coarse PEEC model, but if more demanding, other shapes, such as triangles, must be added to count for the edge and proximity effects. Consequently, the expanding and testing functions used to discretize MPIE will differ, and the loss calculation over these irregular shapes will also change.

The third aspect that needs to improve is the PEEC algorithm. So far quasi-static approximation is adequate, but loss on radiation and surface waves are expected by quite a few RF designers. Therefore MOR incorporating full-wave PEEC algorithm can be an encouraging improvement in the future.

## **AUTHOR'S PUBLICATION**

**Hai Hu**, Jie Wang and Ke-Li Wu, "Physical model order reduction for multilayer lossy RF embedded passives," accepted by *2006 Asia-Pacific Conference*, Japan, Dec. 2006.





CUHK Libraries



004359261